Defining the 3D geometry of thin shale units in the Sleipner reservoir using seismic attributes.

Ponfa Roy Bitrus, David Iacopini, Clare E. Bond

Department of Geology and Petroleum Geology, University of Aberdeen, Aberdeen, AB24 3UE, UK.

*Corresponding Author (e-mail: prbitrus@abdn.ac.uk, +447854859911)

Abstract

Defining the 3D geometry and internal architecture of reservoirs is important for prediction of hydrocarbon volumes, petroleum production and storage potential. Many reservoirs contain thin shale layers that are below seismic resolution, which act as impermeable and semi-permeable layers within a reservoir. Predicting the storage volume of a reservoir with thin shale layers from conventional seismic data is an issue due to limited seismic resolution. Further, gas chimneys indicative of gas migration pathways through thin shale layers, are not easily defined by conventional seismic data. Additional information, such as borehole data, can be used to aid mapping of shale layers, but making lateral predictions from 1D borehole data has high uncertainty. This paper presents an integrated workflow for quantitative seismic interpretation of thin shale layers and gas chimneys in the Utsira Formation of the Sleipner reservoir. The workflow combines the use of attribute and spectral analysis to add resolution to conventional seismic amplitude data. Detailed interpretation of these analyses reveals the reservoirs internal thin shale architecture, and the presence of gas chimneys. The comprehensive interpretation of the reservoirs internal structure is used to calculate a new reservoir storage volume. This is done based on the distribution of sand and interpreted shale layers within the study area, for this active CO_2 storage site.

Keywords:

Seismic, Reservoir, Thin shale beds, Seismic attributes, Utsira Formation, CO_2 storage, Sleipner.

Highlights:

- New seismic interpretation of the internal reservoir geometry of the Sleipner field.
- Seismic attributes inform a detailed interpretation of the geometry and distribution of thin shale layers.
- Fluid-flow features are identified using multi-attribute analysis.
- A new storage volume of 1.05 x 10^9 m^3 is calculated for the Sleipner CO_2 storage site from the interpretation.

1.0 Introduction

The external and internal architecture of a reservoir can affect overall reservoir efficiency (Miall, 1988; Wu et al., 2007; Ambrose et al. 2008; Ran et al., 2014; Baker et al., 2015). Amplitude data is the fundamental seismic data type used for interpretation and reservoir mapping. Attribute analysis using different waveform properties can be combined with an amplitude interpretation to reveal detailed reservoir characteristics not identified in amplitude data (Liner, 2004; Chopra and Marfurt, 2006; Eduardo and Matos 2013). Seismic image processing utilising trace attributes to define reservoir architecture and heterogeneity is routinely carried out within the petroleum industry. Trace attributes are used to improve characterisation of features such as channels, turbidite sequences and gas chimneys within reservoirs. The additional information obtained can be used to improve reservoir volume predictions and enhance volume recovery (Mahapatra, 2006; Philips and Zhang, 2009; Felifel et al., 2014).

Seismic attribute analysis has recognised limitations (Marfurt and Alves, 2014). Some of the limitations result from the acquisition and incorrect time migration of data affected by fast lateral velocity change, while others are associated with seismic attribute algorithm design (Chopra and Marfurt, 2007; Marfurt and Alves, 2014). Trace attributes in most cases exploit stacked seismic waveform properties to track patterns. These patterns are defined by the phase and contrast of impedance variation and are used to characterise the reservoir (Taner, 1979). Unless trace attributes are calibrated with petrophysical information, wireline data or synthetic and inversion modelling data, they are of limited use in tying geophysical response to geological feature (Connolly, 1999).

Complex trace attributes have been used to define quantitatively the characteristics of wavelets such as dominant frequency and stratigraphic variables that can be directly related to bed thickness (Robertson and Nogami, 1984). Hence, attribute analysis can aid the interpretation and reconstruction of thin shale layers that are below the seismic amplitude tuning thickness of $\lambda/4$, which defines the vertical resolution of a seismic image (Robertson and Nogami, 1984; Sheriff and Geldart, 1995). Here we apply analysis of complex trace attributes to define detailed reservoir architecture that could not

be identified in seismic amplitude analysis. We present a workflow that combines the use of well data, seismic interpretation and image processing, to map the 3D reservoir architecture of thin shale layers and to identify vertical sedimentary fluid flow features – gas chimneys, within the reservoir units of the Sleipner field, Norway.

2.0 The Utsira Formation of the Sleipner Field

This paper uses the stratigraphic heterogeneity of the Utsira Formation reservoir within the Sleipner field as a case study to test our seismic attribute analysis workflow (figure 1). The Sleipner Field is proximal to the UK - Norway median line (Nicoll, 2012), with the Cenezoic Era Utsira reservoir covering an area approximately 450 km in length from north to south with an east to west width of around 40 – 90 km (figure 1) (Zweigel et al., 2000). The geology and stratigraphy of the Cenozoic Era for the Sleipner field area has been documented extensively by a number of authors, see Galloway, (1981); Isaksen and Tonstad, (1989); Jordt et al., (1995); Zweigel et al., (2004); Chadwick et al., (2004); and Gregersen and Johannessen, (2007) for further details. The Sleipner area is defined by two main groups: the Hordaland groups and the Nordland group. The Hordaland Group shales (Eocene to Early Miocene) underlie the Utsira Formation and are described as Mudstone dominated units (Head et al., 2004). The Nordland Group marine and glacial sediments (Pliocene - Pleistocene) form the overburden (figure 2a) (Head et al., 2004). The Sleipner study area is located at the Southern depocentre of the Utsira Formation, where its maximum thickness is ca.300 m (figure 1b).

The Utsira Formation is a shallow marine sandstone interpreted to have been deposited both as a contourite drift and tidal sand ridge (Rundberg, 1989; Galloway et al., 1993; Gregersen et al., 1997). The Utsira Formation has a thickness of about 200 – 300 m and is a saline aquifer of Miocene age within the Nordland Group in the North Sea (Isaksen and Tonstad, 1989; Gregersen et al., 1997; Fyfe et al., 2003; Zweigel et al., 2004; Chadwick et al., 2004)

The internal reservoir architecture of the Utsira Formation is controlled by the distribution of interbedded thin shale layers within a sandstone body (Miall, 1980; Ambrose et al., 2008). The thin

shale layers act as baffles and intra-reservoir seals with variable permeability (Lindeberg, et al., 2000; Chadwick et al., 2000, Kirby et al., 2001; Arts et al., 2004a, b; Arts et al., 2008). The Utsira Formation has been used to store CO_2 for over a decade, with approximately 15 million metric tonnes of CO_2 sequestered to date (Chadwick et al., 2014). Migration of the injected CO_2 within the reservoir has been monitored by 3D seismic time-lapse survey (Chadwick et al., 2008). Previous research suggests that higher permeability pathways existed in the Utsira Formation prior to CO_2 injection, these high permeability pathways are referred to as gas chimneys (Gregersen et al., 1997; Chadwick et al., 2004; Zweigel et al., 2004). This assertion is supported by the evidence of mud volcanoes as a source of expulsed gases from the base of the Utsira, and the presence of high seismic amplitude anomalies described as paleogeogas in the Pliocene units of the study area by Løseth et al., (2009) and Jackson and Stoddart, (2005).

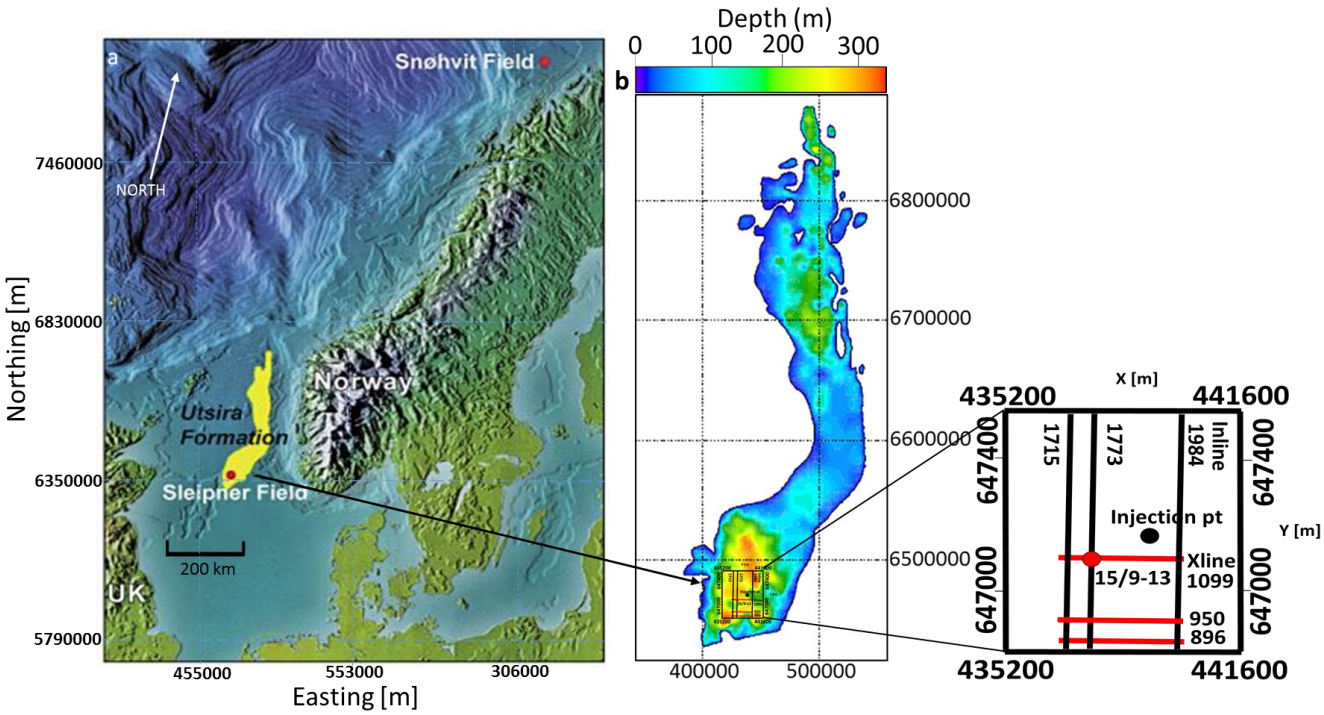

Figure 1: The location and extent of the Utsira Formation in the North Sea a) Topographic map of the North Sea, the Sleipner Field is marked by a red dot, with the extent of the Utsira Formation highlighted in yellow. Source: (Arts et al., 2008); b) Isopach thickness map of the Utsira reservoir sand showing the thickest part in the southern depocentre, colour scale in meters (sand thickness). Source: (Kirby et al., 2001);Inset box shows the survey extent of 3D seismic cube showing well 15/9-13, CO_2 injection point, and inline (black lines) and crosslines (red lines) used in figure 2, 8,14 and 19.

2.1 Stratigraphy of the Sleipner Field

The Stratigraphy of the main reservoir unit and cap rock for the Sleipner Field, is outlined in figure 2 and described below:

Basal Shales - Hordaland Group Shales (Mid-Miocene ~ 12 – 15.5 Ma) characterised by polygonal faulting, soft sediment deformation and numerous mounds interpreted as mud diapirism (Cartwright, 1994; Chadwick et al., 2004 and Jackson and Stoddart 2005).

Reservoir - Nordland Group Utsira Sand (Mid-Miocene to late Pliocene ~2.5 – 12 Ma) is defined as a basin restricted sand of marine origin, comprised of stacked low relief overlapping mounds that are interpreted as individual fan lobes (Gregersen et al., 1997). The Utsira Sand is a seismically resolvable unit with a sharp top and base and is interbedded with over 10 intra-reservoir mudstone or shale layers. Each shale layer has an average thickness of ~1.3 m as interpreted from gamma ray and neutron density logs (Zweigel et al., 2000; Holloway et al., 2000; Chadwick et al., 2004). Core analysis of the Utsira Sand gives porosity estimates that range from 27% to 31%, locally up to 42%, with a permeability of 1 – 3 Darcy (Holloway et al., 2000; Chadwick et al., 2002; Arts et al., 2008).

Cap rock - Top Nordland Group Mudstones (Gelasian- Pleistocene to Holocene sequence, ~2.5 – 0 Ma), also known as the Pliocene units, overlie the Utsira top shale and represents a deep transitional water environment (Head et al., 2004). They represent the upper boundary of the sequence and have been sub-divided stratigraphically into three units by (Gregersen and Johannessen, 2007). The first is the Lower Seal or Shale Drape (Gelasian ~1.8 – 2.5) which is 50 – 100 m thick , and forms part of the basin-restricted shale units (Chadwick et al., 2004; Head et al., 2004; Nicoll, 2012). The Middle Seal (Calabrian ~70 – 150 m) made up of stratigraphic features such as clinoforms, which can act as higher permeability pathways for reservoir fluids and gases (Fyfe et al., 2003; Chadwick et al., 2004; Head et al., 2004; Nicoll, 2012). High seismic amplitude anomalies described as palaeo-gas (Nicoll et al., 2010) are seen on 3D seismic data within this middle ‘seal’ (figure 2b). The high amplitude anomalies are characterised by higher velocity, log density and resistivity measurements when compared to the underlying and overlying units (Heggland, 1997; Holloway et al., 2000; Head et al., 2004). Finally the

Upper Seal (Pleistocene to Holocene ~1m -70m) is characterised by glacio-marine clays and glacial tills (Graham et al., 2007).

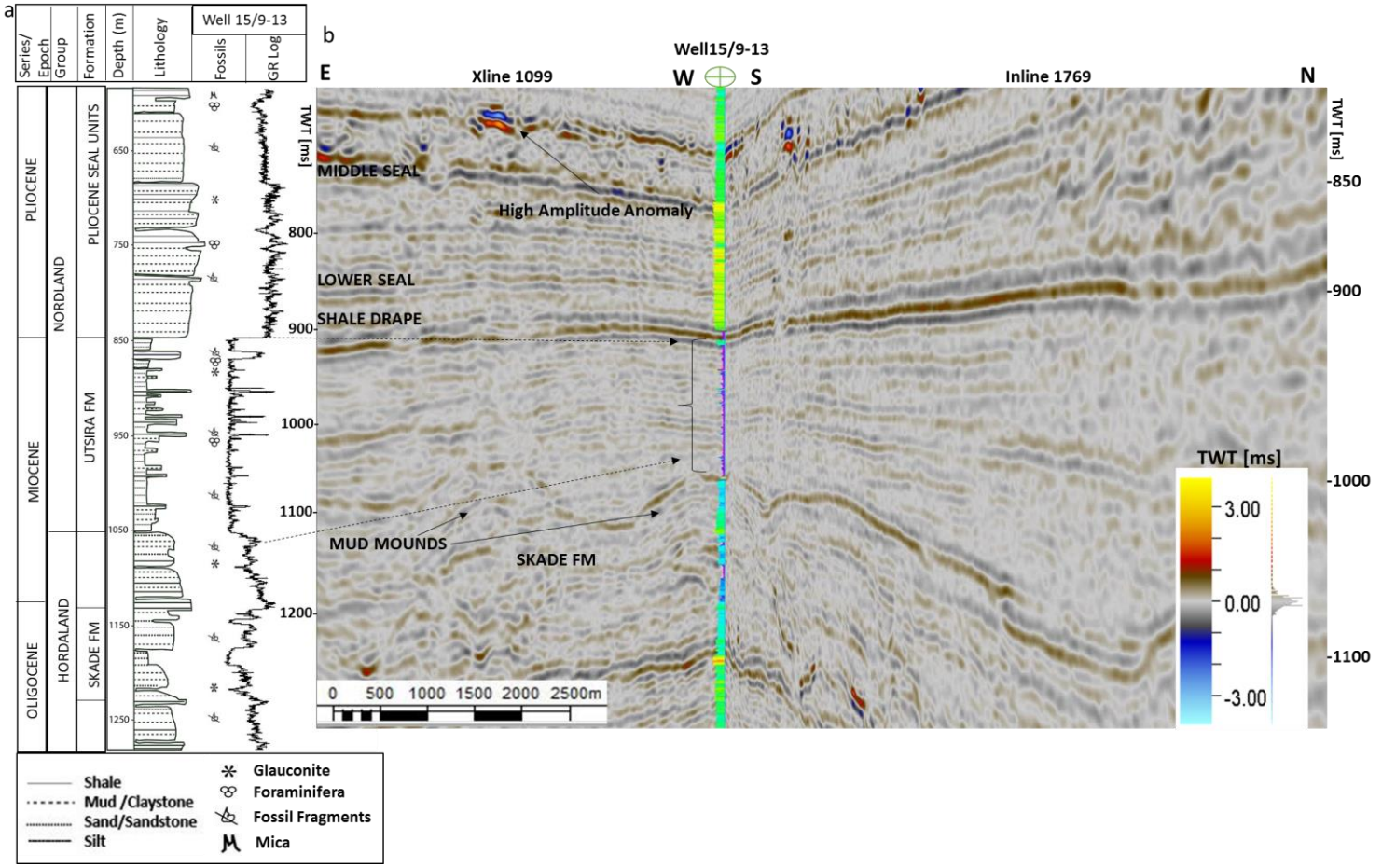

Figure 2: Schematic sedimentary log, well log and seismic data from the study area. a) Lithological log, depth, age and GR log of well 15/9-13. b) Inline and crossline display from the 3D seismic data in the study area (inline 1769 E-W and crossline 1099 S-N tied to well 15/9-13). The seismic image is displayed in a normal amplitude TWT spectrum. Well 15/9-13 is displayed as a gamma ray log, curved fill colour indicating different formations and lithological groups.

3.0 Methodology

The seismic dataset utilised is a 1994 3D seismic cube of the Sleipner field covering a 3 x 7 km area, with a vertical extent of 0-2000 ms. Survey acquisition parameters include the use of two seismic sources with a volume of 5.57 x 10^{-2} m^3, a source tow depth of 6 m, length 16 m and width 20 m and a near offset of 195 m. The seismic survey cube was processed using an amplitude preservation process and migrated using Kirchhoff prestack time migration (PSTM) (Furre, 2013). A single well; 15/9-13 within the study area is used with its associated wireline logs (figure 2a).

The workflow is summarised in figure 3, each element is discussed in turn in the text. The software packages used for seismic analysis and interpretation were Petrel® (version 2013/2014) and Geoteric (version 2013).

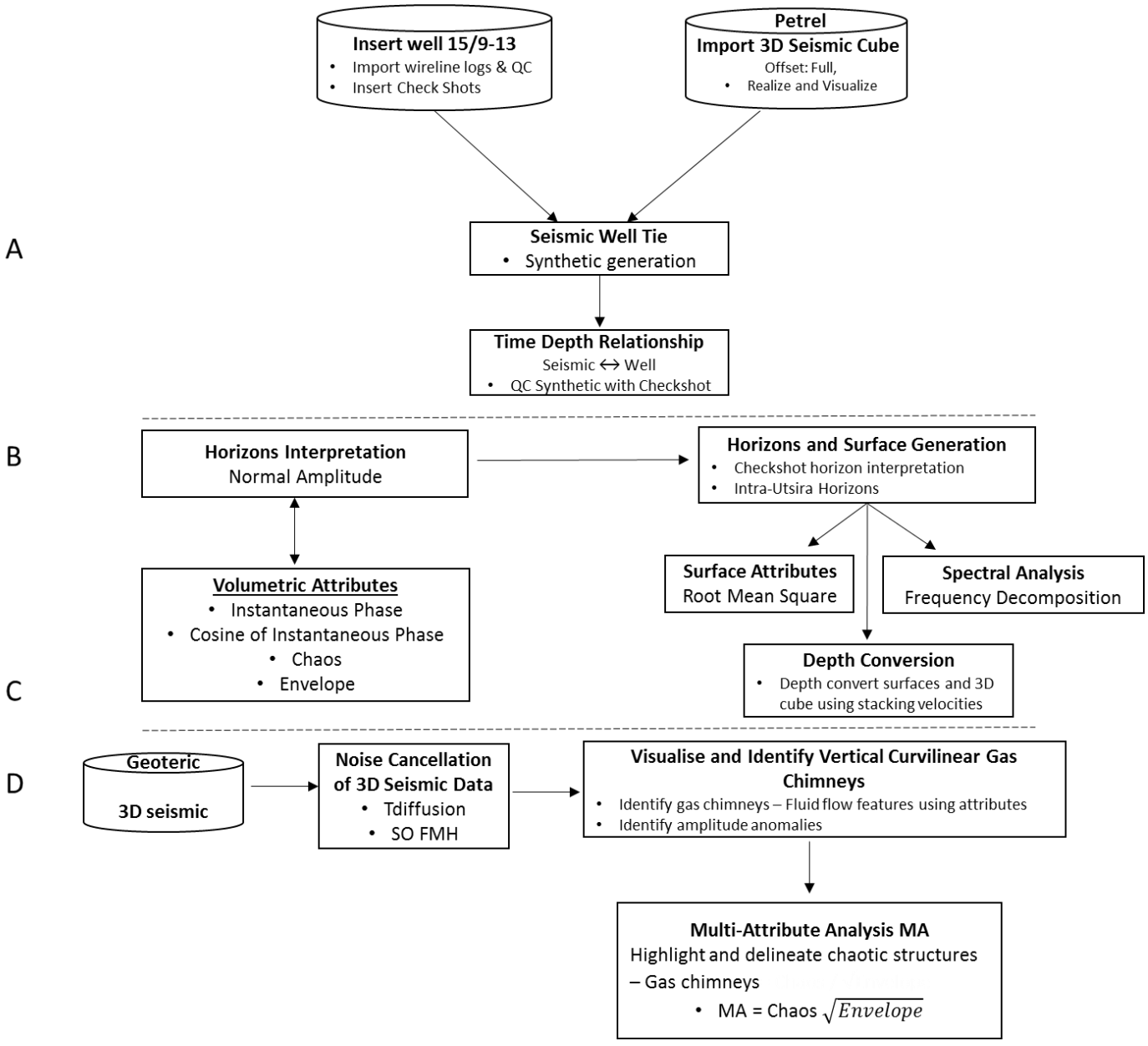

Figure 3: Workflow diagram outlining the methodology followed in analysing and Interpreting horizons and identifying sedimentary features imaged in the 3D seismic data. (Bold numbers on the left indicate figure parts referred to in the text).

Prior to seismic interpretation (figure 3-A), it is important that synthetic traces are computed by convolving the reflection coefficient (sonic logs obtained from well 15/9-13) with the extracted wavelet from the seismic dataset, so they are aligned with the corresponding event in the seismic data

(figure 4). The seismic well allows the seismic waveforms to be related to the stratigraphic and petrophysical properties of the reservoir.

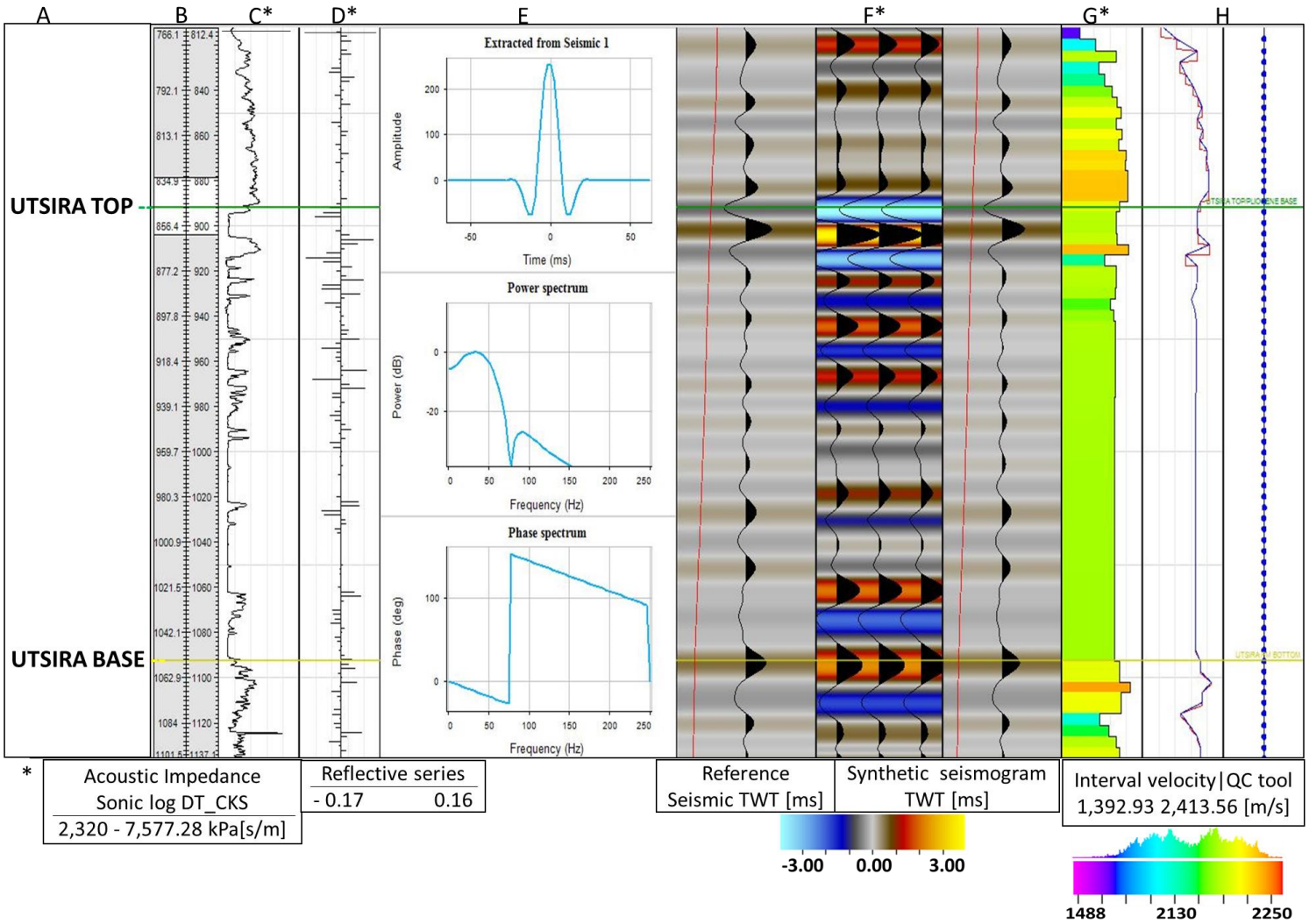

Figure 4: Seismic well tie and synthetic seismic generation from well 15/9-13 and 3D seismic data, A) Well tops of Utsira Formation reservoir, B) TVD (m) vs TWT (ms) correlation, C) Acoustic impedance – sonic log used for reflectivity calculation D) Reflection coefficient from the reflectivity series, E) Corresponding ricker wavelet extracted from seismic dataset for use, F) Synthetic seismogram generated compared against corresponding reference seismic trace from the study area, G) Interval velocity displayed as a graphical log with legend beneath, H) Interval velocity quality control (QC); input interval velocity (red line) vs output interval velocity (blue line) and synthetic seismic drift curve for time shifts applied.

When working with thin beds on a zero-phased data, the actual number of thin beds may not correspond to the number of reflections in the seismic data. Closely spaced thin bed reflectors, less than or equivalent to one-quarter thick (λ/4) of the seismic wavelength, will produce amplitude reflections. These amplitude reflections will be imaged as individual reflections and are due to constructive interference from seismic reflectors (figure 5). Each thin bed is therefore interpreted

based on the thickness of the bed as it relates to the wavelength and the acoustic impedance contrast between the interpreted bed and the adjacent strata. Thin shale layers with relatively high acoustic impedance contrast can be seismically visible, as can thick layers with low acoustic impedance contrast. The seismic amplitudes of the interpreted seismic data are affected by the changes in acoustic impedance which is associated with changes in reservoir lithology, porosity and fluids, and changes in tuning thickness. To avoid the risk of ambiguous interpretation of seismic thin bed layers, the seismic amplitude must be properly tied to a well data (Mavko *et al*., 2010).

Horizons were interpreted from the 3D seismic data in Petrel® (figure 3-B). Twelve horizons were interpreted: the Utsira base, Utsira top and ten Intra-Utsira horizons. Interpretation was carried out by manually cross tying and picking seismic reflectors on inline and crosslines, with a grid increment spacing of 2 x 2 (25 m x 25 m).

Two volumetric complex trace attributes were used to aid horizon interpretation of the Intra-Utsira horizons that define the thin shale layers within the reservoir. The complex trace attributes used were the Instantaneous Phase and the Cosine of Instantaneous Phase. The attributes can be displayed as a colour spectrum that enhances the visual display of the seismic image for interpretation of the reservoir's stratigraphy (Taner, 1979; Purves, 2014).

Wedge model analysis and it's concepts best explain the relationship between seismic resolution, detection limits and tuning phenomena and the potential impact of the use of complex trace attributes in interpreting thin beds in seismic sections (Robertson and Nogami, 1984). The vertical resolution of the Utsira Formation is ca. 14.18 m. This means that the intra-reservoir shales (baffles) and sandstone (high permeability pathways) are not easily resolvable in the 3D seismic dataset used, as they are below the seismic tuning thickness. Therefore, an understanding of the wedge model is key to developing a technique for thin bed interpretation. In figure 5, the shale above and below a thin bed of sand have the same acoustic impedance. Thus the reflection coefficient at the top and bottom of the bed will have the same magnitude but reflect opposite wiggle signs (Brown, 2004). The two wavelets exist as separate waveforms that are overlapping, hence a seismic resolution of λ/4 (figure

5). The only indication that a bed increases or decreases in thickness across the wedge is the difference in time between the top reflection and base reflection of the bed (Hart, 2012). The use of complex trace attributes enhances imaging of thin beds as it highlights properties of the normal amplitude data and quantitatively defines wavelet character, like dominant frequency and stratigraphic variables that relate to the thickness of a formation (Taner, 1979; Robertson and Nogami, 1984).

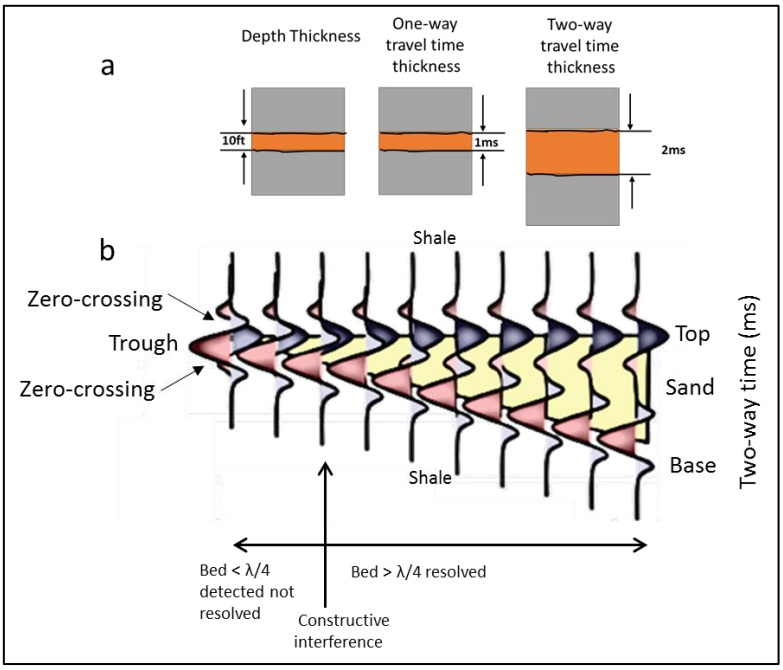

Figure 5: The wedge model thin bed analysis concept. a) Thickness measurement comparison of a one way travel time to a two-way travel time, b) Schematic wedge model of individual seismic reflections generated based on reflection coefficients of the top and base of the wedge.The shallow clastic Utsira Sand saturated in saline water will have a lower acoustic impedance than its embedding shale (Chadwick and Eiken, 2013).The acoustic impedance of the wedge and the shale layers above and below the wedge do not change, hence the amplitude of the reflections do not change. To the left of the wedge, there will be interference between the top and base reflections.

The Instantaneous Phase (IP) attribute is amplitude invariant and is used to effectively show continuities in sequence boundaries and bed interfaces to reveal stratigraphic patterns of onlap and downlap (Daber et al., 2007). The IP is expressed as:

$$\varphi(t) = \tan^{-1}[(g(t)/f(t)] \qquad (1)$$

Where φ(t) Instantaneous Phase is mathematically expressed as the real *f(t)* and imaginary part *g(t)* of a seismic trace (Daber et al., 2007)

The Instantaneous Phase assigns the same colour to the real trace, such that the phase angle that corresponds to each peak, trough and zero crossing can be followed trace by trace (Taner, 1979). The Cosine of Instantaneous Phase is dephased by 180^{o} degrees to the IP. It is also often referred to as the normalised amplitude as the output data is scaled from -1.0 to 1.0. This normalisation represents the seismic reflectors as a grey scale, white to black.

The Cosine of Instantaneous phase is expressed as:

Cosine of Phase = Cos (φ (t)) (2)

The Cosine of Instantaneous Phase (Cosine of Phase) is used to guide interpretation in poorly resolved areas of a 3D seismic data set, as it is effective in displaying lateral continuity and stratigraphic terminations (Taner, 1979; Chora & Marfurt, 2007)

Combining multiple seismic attributes in a visualisation of seismic image data often reveals more detail for interpretation than visualisation of the individual attributes. In our methodology we visualise the complex trace attributes (Instantaneous Phase and the Cosine of Phase) interchangeably with the normal amplitude data to identify and interpret thin shale beds, and their continuity, across the Utsira Formation within the 3D seismic cube (figure 6).

Other attributes combined and used include Chaos and Envelope attribute. Chaos is a stratigraphic attribute that maps seismic reflector chaos, defined as the level of disorganisation of the orientation in the estimated dip and azimuth of the data in a selected 3D window (Iske and Randen, 2005). It is essentially a gradient structural tensor algorithm (Marfurt et al., 1999). In stratigraphic analysis the level of chaos in the attribute often increases in areas affected by fluid migration and intrusive bodies such as salts and igneous intrusions that disrupt planar stratigraphy. Features such as faults, channel infill and reef textures often correspond to areas with a chaotic seismic response, and are identified as areas with a low signal consistency (Marfurt et al., 1999).

Envelope, also known as instantaneous amplitude or reflection strength is defined as the total energy of a seismic trace. Envelope is phase independent and envelopes the waveform associated with the

positive phase rotation from 0° to 360° (Daber et al., 2007). Mathematically it expresses the real *f(t)* and imaginary part *g(t)* of a seismic trace (Daber et al., 2007), given as:

Envelope = $[(f^2(t) + g^2(t)]^{½}$ (3)

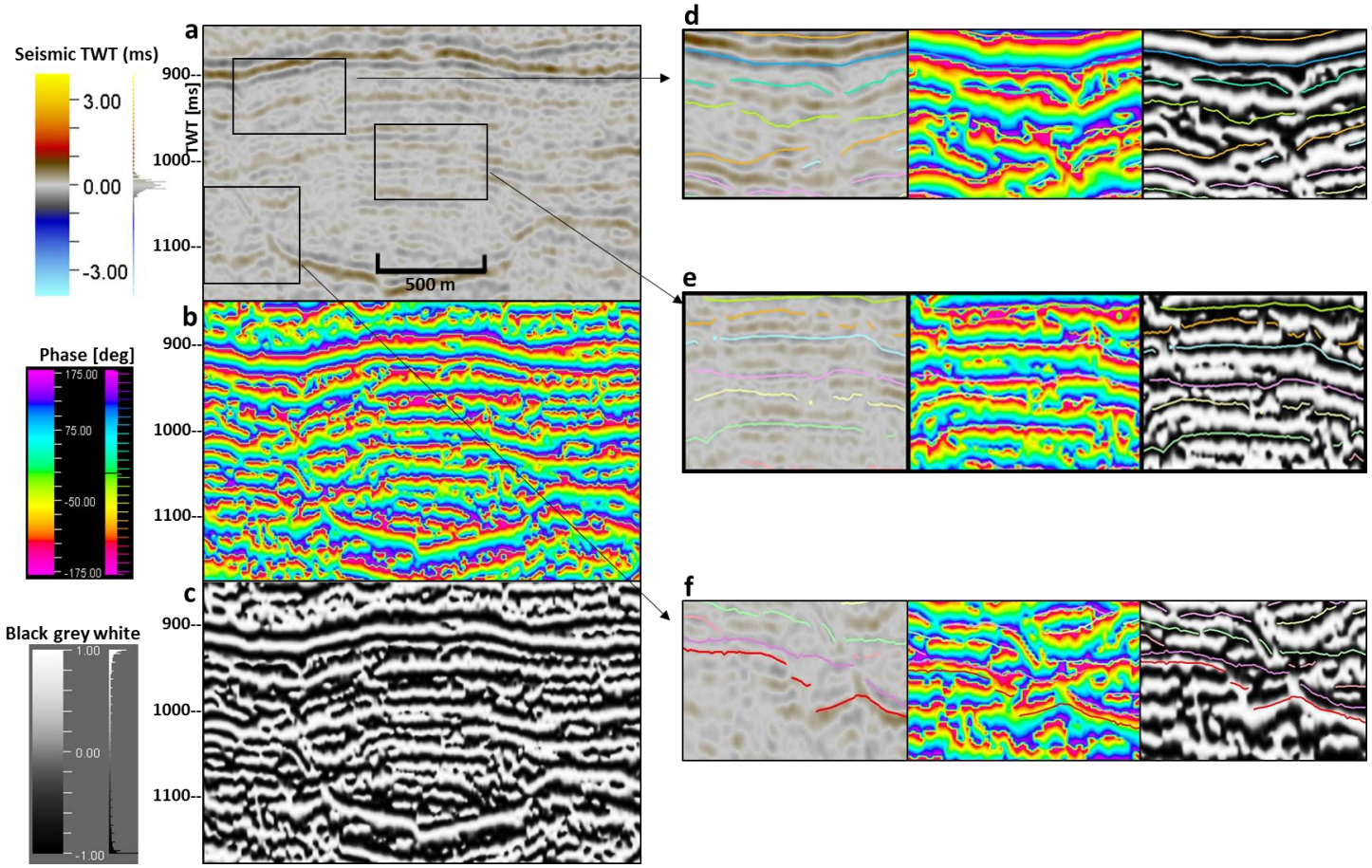

Figure 6: Comparison of the normal amplitude and complex trace attribute responses of a seismic cross-section selected from the 3D seismic cube. Visualisations of the seismic cross-section are: a) normal amplitude, b) Instantaneous Phase c) Cosine of Phase. Enlarged areas, boxes in a. are shown in d, e and f where reflectors and interpreted horizons show d) a discontinuous zone e) Phase reversal and chaotic reflection zones, and f) local depression zone. For the Instantaneous Phase the colour scale is green –0 degrees, through to purple +/- 180 degrees. While the colour scale for the Cosine of Phase is +1 white to -1 black.

The Root mean square (RMS) attribute, also referred to as the quadratic mean measures the amplitude response over a seismic dataset. The RMS attribute places an emphasis on the variation in acoustic impedance over sample intervals (Daber et al., 2007). This means that a bed thickness above a seismic resolution of λ/4 will have the brightest RMS value, while a bed thickness less than or equal to λ/4 will have a lower RMS value (Chopra and Marfurt, 2007; Avseth et al., 2010). The RMS attribute is expressed as:

RMS = $\sqrt{\frac{\sum_i^n amp^2}{k}}$ (4) or $\sqrt{\frac{X_1^2 + X_2^2 + \cdots + X_n^2}{n}}$ (5)

Equations 3 and 4 represent the square root of the sum of the squared amplitudes (amp or X) divided by the number of live samples (k or n) (Daber et al., 2007). The RMS attribute was used to empirically enhance anomalies or isolated features within the interpreted horizons by the use of amplitude response as described by Kragh and Christie, (2002) and Daber et al., (2007).

Results from spectral analysis are used to resolve and detect the variability in impedance of subsurface rocks to determine the thickness of the horizons and the layer stacking. Spectral decomposition analysis also known as frequency decomposition (FD) is the process of analysing seismic signals through Fourier analysis into its constituent frequencies (Henderson et al., 2007; McArdle and Ackers, 2012). FD isolates discrete frequencies from a spectrum generated from the 3D seismic data which is used to identify and discriminate between geological expressions of a reservoir (Partyka et al., 1999; Hall and Trouillot, 2004). The FD method used in this study utilises a colour blending tool to co-visualise three discrete frequency outputs as an RGB (Red, Green, and Blue) colour response (figure 7) and it is expressed as:

$C_{out}(x,y,z) = C(I_R(x,y,z), I_G(x,y,z), I_B(x,y,z))$ (6)

Where $C_{out}(x,y,z)$ is the output image with colour assigned RGB, $I_R(x,y,z)$, $I_G(x,y,z)$, $I_B(x,y,z)$ determined from voxel values at a point (x,y,z).

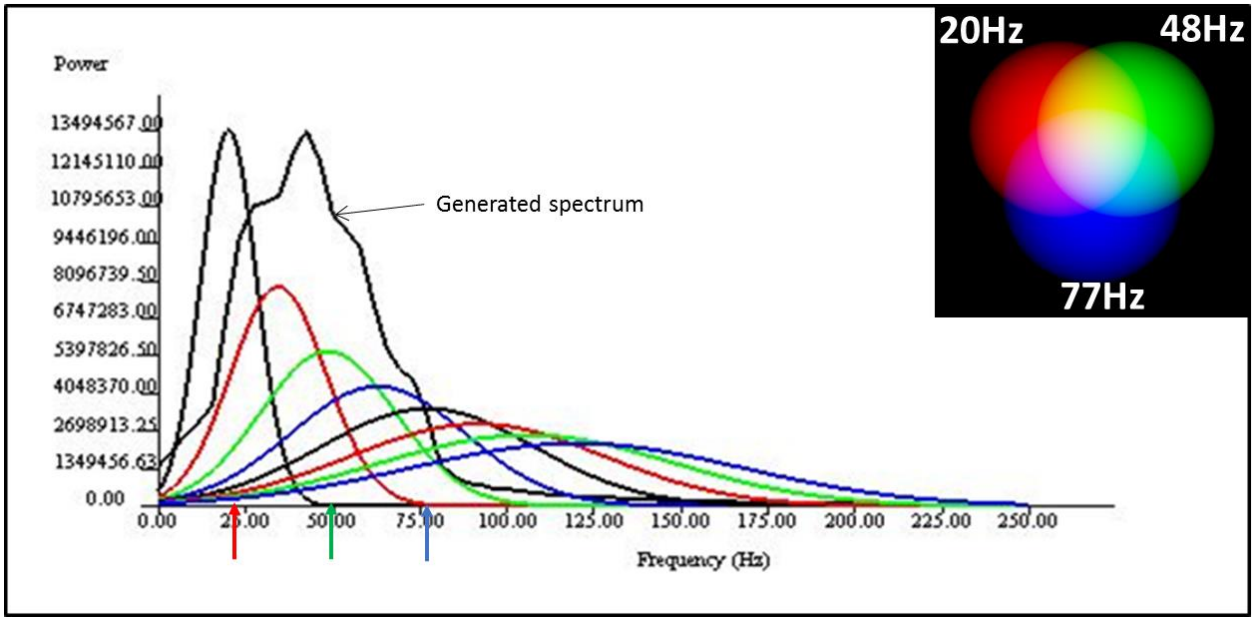

Figure 7: Generated spectrum from the 3D seismic data and the min, med and max (20Hz, 48Hz and 77Hz respectively) frequencies used within the generated spectrum. Insert is the RGB colour blend scale bar; White or light grey colour indicates a strong response from all three frequency channels while a black or dark grey colour indicates weak response from all three channels.

Three magnitude frequencies were chosen from the generated spectrum (figure 7) at 20Hz, 48Hz and 77Hz (Red Green and Blue respectively). The frequencies were blended and co-visualised on the interpreted seismic horizons to reveal variability in the petrophysical properties of the horizon. A strong response from all three frequency channels will display a white or light grey colour whereas a weak response from all three will give a black or dark grey (Chopra et al., 2006). A black or dark response represents high frequencies that can be the result of thin beds or discontinuous beds below seismic resolution that are out of tune with the selected frequencies. Low frequency (seen in red) represents the thick packages while intermediate frequencies highlight the discontinuities and transitions between the higher and lower frequencies. Continuous thin beds in a formation often leads to patchy interference and an increase in the high frequency while decreasing the seismic wavelet of the low frequency components (Chopra and Marfurt, 2015).

Detailed horizon mapping of the shale layers in the Utsira Sand Formation was completed in seismic TWT (two way travel time). It is therefore necessary to convert the 3D seismic and interpreted

horizons to depth (m) (figure 3-C), to produce a depth and thickness map of the reservoir. Such maps are commonly used in volumetric estimations of petroleum reservoirs.

The depth conversion was undertaken utilising interval and average velocities converted from stacking velocities using the Dix equation.

$$V_{int} = [(t_2 V_{RMS2}^2 - t_1 V_{RMS1}^2) / (t_2 - t_1)]^{½} \quad (7)$$

Where V_{int} = Interval Velocity, t_1 = traveltime to the first reflector, t_2 = traveltime to the second reflector, V_{RMS1} = root-mean-square velocity to the first reflector, V_{RMS2} = root-mean-square velocity to the second reflector. Well 15/9-13 was used to quality check the depth converted model. The depth converted horizons are compared to the TWT horizons and an RMS attribute of the same in figure 16, to highlight the changes in morphology of the horizon.

Gas chimneys are seen across the 3D seismic data (figure 3-D), defined by low amplitude chaotic and discontinuous patterns that outline vertical curvilinear features. To highlight and interpret these gas chimneys, we have employed noise cancellation in combination with multiple-attributes to visualise the 3D seismic data.

Noise cancellation was carried out on the 3D seismic data to eliminate seismic artefacts resulting from the acquisition footprint, which can be mistaken for sedimentary features. The noise cancellation process employs an algorithm that stays true to the orientation of the structural dip and azimuth of the data. Two noise cancelling filters were used in the noise cancellation process, they were the anisotropic edge preserving diffusion filter (Haralick, 1984) and the structurally oriented finite median hybrid (SO FMH) filter (Iacopini et al., 2012).

The anisotropic edge preserving diffusion filter improves the continuity of the amplitude reflectors by aligning itself automatically to the dominant structure whilst preserving stratigraphic discontinuities (Gilani, 2013). Applied to 3D seismic data, it improves the lateral continuity of the stratigraphy in areas that at first appear chaotic by filtering random noise such as seismic artefacts. The SO FMH filter targets coherent noise that can result from the acquisition and migration footprint, whilst preserving subtle details like structural edges and sharp dip changes within the data (Iacopini et al., 2012; Gilani,

2013). Application of the two filters enhances the visual display of the 3D seismic data around the edges of the gas chimneys, by eliminating the presence of random and coherent noise within the data. The resulting noise cancelled 3D seismic data was used as input data for multiple attribute analysis to delineate and highlight gas chimneys.

The multiple attribute analysis combines two volumetric attributes such that they are applied as a single attribute on the 3D seismic data (Guo et al., 2008). The multiple attribute analysis has the potential to highlight and reveal patterns otherwise obscured by chaotic seismic reflections and areas of low amplitude, in this case – gas chimneys.

The Multi-Attribute [MA] used is expressed as

$$MA = Chaos / \sqrt{Envelope} \qquad (8)$$

4.0 Results and Interpretations

The application of complex trace attributes and multi attributes to aid the interpretation of 3D seismic data brings out the details of the geometry of the subsurface reservoir (figure 8).

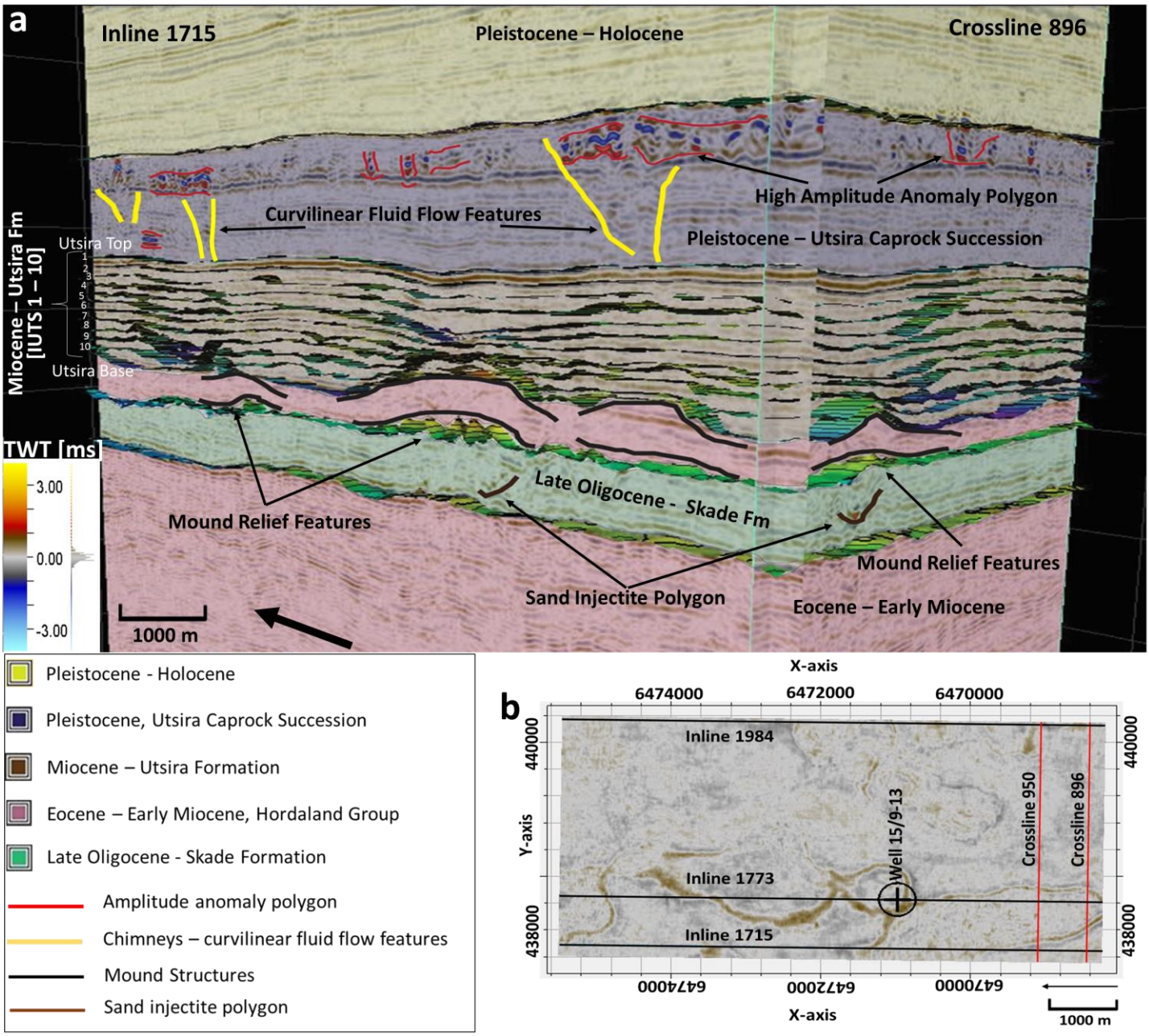

Figure 8: 3D seismic cube of the study area showing a summarised view of the stratigraphic groups; a) Inline 1715 and crossline 896 displays the Nordland Group (Miocene Utsira Formation and the Pliocene Units) and the Hordland group (Late Oligocene - Skade Formation). Beneath the Utsira base are mud relief mounds down to the Skade Fm top. The Utsira Formation showing the edges of the interpreted intra-reservoir shales labelled IUTS1 down to IUTS10 and the Utsira top. Seismic anomalies are seen in the Pliocene unit's ca. 200 – 300 m above the mud mounds in the Utsira base. b) A 2D map view of the study area showing the location of well 15/9 – 13 and seismic Inlines 1715, 1773 (figure 19), 1984 (figure 14) and crosslines 896 and 950 (figure 14) on time slice 1102 at the base of the Utsira Formation.

The base of the Utsira reveals mud diapirs – MRF1 to MRF6, which are distinguished by FD and RMS on the Utsira base horizon (figure 9). Relief features can also be seen in the Utsira top horizon (figure 10 and 11) and the IUTS horizons (figure 15). Thickness variations of the sand layers between the

interpreted thin shale layers can be seen in table 1 and figure 14. Table 1 is a summary of the interpreted horizons and the difference in the sand thickness in TWT (ms) and depth (m) between shale layers. The values were used to calculate the amount of available pore space in the Utsira Formation study area. The total average pore volume of 1.05 x 10^9 m^3 was calculated assuming an average porosity of 30 % from a total volume of 3.51 x 10^9 m^3.

No.	Surface	Surface Depth Range TVDSS	Surface Thickness Map. TWT (ms) thickness range between Interpreted Surfaces)	Surface Thickness Map. Depth (m) thickness range between Interpreted Surfaces)
1	Utsira top	834-880	20 – 36 (Utsira T – IUTS1)	15 – 27.50 (Utsira T – IUTS1)
2	IUTS1	865-910	15 – 26 (IUTS1 – IUTS2)	10 – 20 (IUTS1 – IUTS2)
3	IUTS2	880-935	15 – 32 (IUTS2 – IUTS3)	11 – 22.50 (IUTS2 – IUTS3)
4	IUTS3	900-965	14 – 35 (IUTS3 – IUTS4)	10 – 25 (IUTS3 – IUTS4)
5	IUTS4	925-980	4 – 35 (IUTS4 – IUTS5)	1 – 25 (IUTS4 – IUTS5)
6	IUTS5	940-1000	10 – 34 (IUTS5 – IUTS6)	7 – 25 (IUTS5 – IUTS6)
7	IUTS6	970-1010	5 – 35 (IUTS6 – IUTS7)	5 – 25 (IUTS6 – IUTS7)
8	IUTS7	990-1036	0 – 35 (IUTS7 – IUTS8)	0 – 27.5 (IUTS7 – IUTS8)
9	IUTS8	1000-1060	0 – 38 (IUTS8 – IUTS9)	0 – 27.5 (IUTS8 – IUTS9)
10	IUTS9	1126-1076	0 – 35 (IUTS9 – IUTS10)	0 – 25 (IUTS9 – IUTS10)
11	IUTS10	1041-1096	0 – 35 (IUTS10 – Utsira base)	0 – 26 (IUTS10 – Utsira base)
12	Utsira base	1046-1116		

Table 1: Showing the interpreted horizons with their surface depth (TVDSS), ranges in surface thickness map in TWT (ms) and Depth (m) between the interpreted horizons.

4.1 Utsira Sand Formation Base

The base of the interpreted Utsira Formation was zero-phased and of normal SEG positive polarity, the base of the Utsira Sand corresponds to the maximum of a peak, with a surface depth (TVDSS)

ranging from 1046 -1116 m (figure 12 and 13). The Utsira base is interpreted to be a sand boundary from its amplitude polarity reflector (figure 12) and wireline logs (figure 13). Where mud diapirs penetrate the Utsira base the amplitude reflectors become disrupted, and are interpreted as thin chaotic beds resulting from diapiric processes (figure 10b and 12); these areas correspond to mapped changes in elevation of the base of the Utsira that show the physical relief of the mud diaper mounds (figure 9a, b). Areas of high relief do not always correspond to a low amplitude RMS signal, suggesting that relief alone does not allow identification of mud diapirism (figure 9). Mound relief feature are observed having a North to South trend (figure 9). Mud diapirs are often geo-spatially associated with concave areas of minimum elevation of the base of the Utsira (figure 9a, b).

Application of RMS attribute and frequency decomposition analysis to the interpreted sand base horizon reveals the amplitude variability that exists within the geometry of the formation. The TWT elevation values of the Utsira base (figure 9 a, b) reveal relief features labelled MRF1 to MRF6. MRF2 despite being identified as high relief feature has a high RMS value (figure 9c) and is therefore not interpreted as a mud diapir. Whereas MRF1, 2, 3, 4 and 5 have lower RMS amplitude responses compared to the surrounding Utsira base and are interpreted as mud diapirs. The frequency decomposition magnitude blend (figure 9d) shows MRF1 as unresponsive to any of the frequencies, while MRF2 – MRF5 have a distinguishable frequency response, this is interpreted as variation in horizon thickness across the study area.

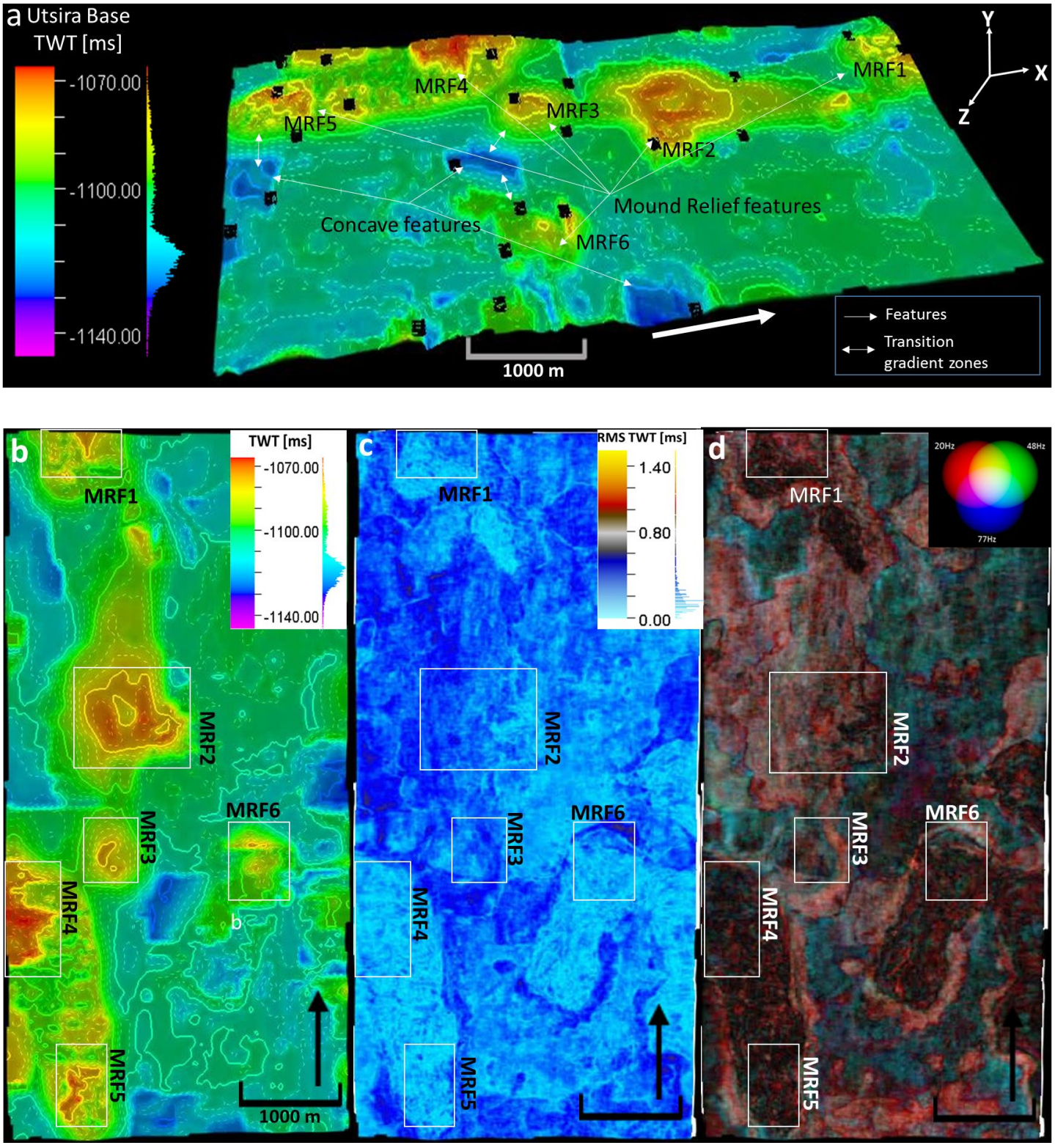

Figure 9: a) 3D Utsira base surface topographic map in TWT [ms]. The 3D map is inclined to show the MRF (Mound Relief Features) and the transition zones into the concave features within the horizon.
b) 2D view of the 3D topographic map of the Utsira base horizon. c) RMS attribute map of the Utsira Base horizon in 2D view. The MRF's have a lower RMS value, due to thin beds disrupted by mud diapirism compared to the lower areas with higher RMS value indicating thicker beds. d) Spectral decomposition RGB frequency colour blend (20Hz, 48Hz, and 77Hz) showing variability in the Utsira base in 2D view. Dark opacity colours displayed

on the MRF's indicate low frequency response, due to low tuning thickness. Intermediate opacity colours between green and blue shows a transition from medium to high frequency content NE of the horizon.

4.2 Utsira Formation Top

The interpreted Utsira Formation top was picked as a zero-phased normal SEG polarity, negative trough reflector with a surface depth (TVDSS) ranging from 834 – 880 m. The Utsira top has a strong continuous amplitude reflection compared to the reflectors beneath (figure 10b, c). Due to its high RMS value compared to the intra reservoir thin shale layers, the Utsira top is interpreted to be a thick shale cap rock overlying the Utsira reservoir (figures 11 and 16). The interpreted Utsira Formation top reveals a slight south – southwest dip, with a distinct relief feature, north – north central extending for ca. 3 km. The relief features have diameters ranging from 1 km to 2 km and heights of ca. 50 m to 100 m (figure 10a). The interpreted horizons as seen from the top of the Utsira form a saddle structure (figure 14a), with gently dipping concave and convex geometries. These geometries are a result of the uplift of the mounds at the base of the Utsira as seen on crossline 1087 (figure 10b). The convex features in the Utsira top to the southeast and southwest of the surface range from ca. 10 -20 m with the largest convex feature at the west side of the surface stretching about 2 km (figure 11a). The concave features could be the result of sagging of the overlying layers surrounding the mud diapirs.

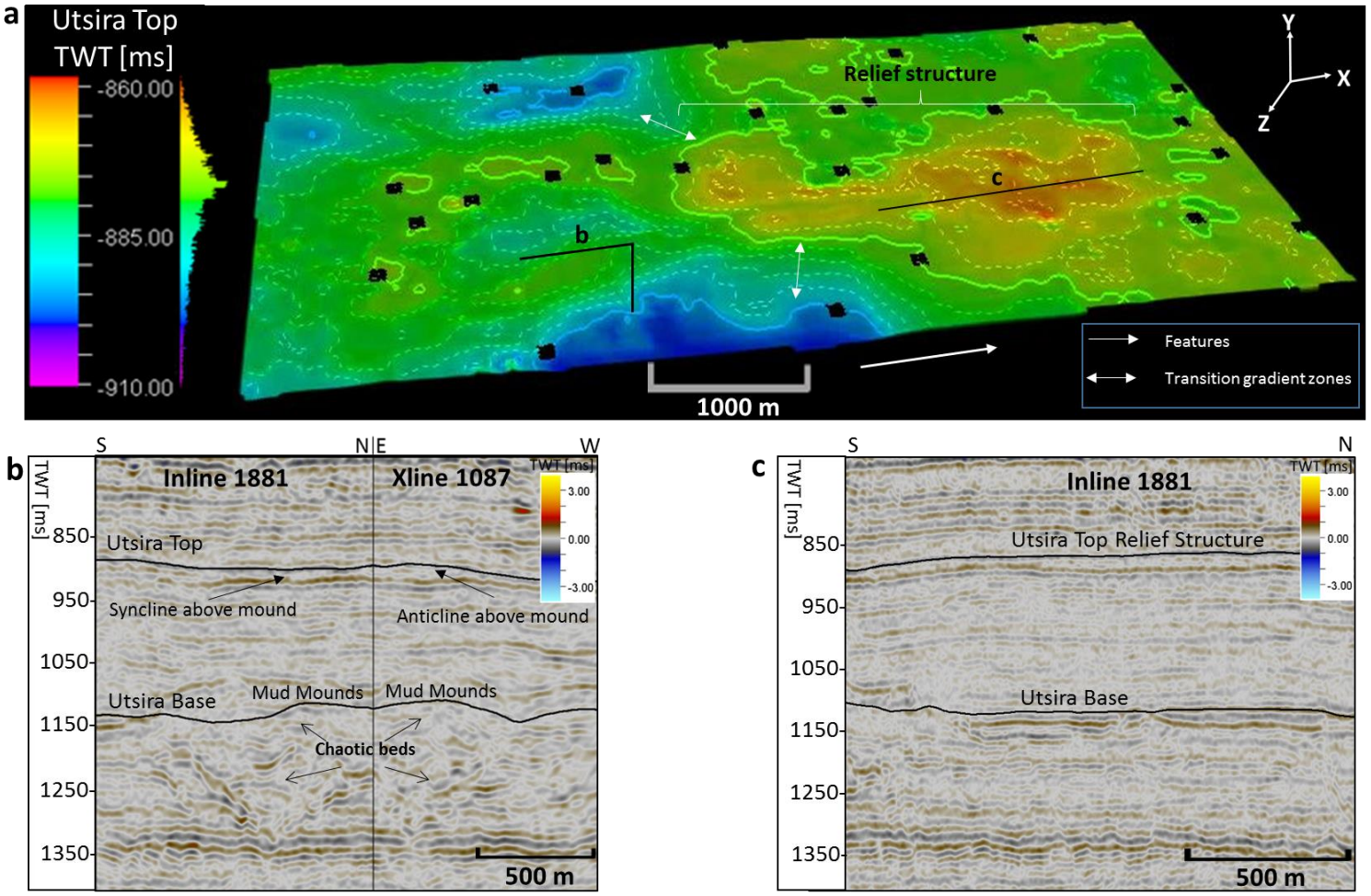

Figure 10: Interpreted Utsira top horizon and seismic cross section across the horizon: a) 3D topographic map in height values [ms] inclined to show the subtle relief structure and concave features across the horizon. Inset are seismic arbitrary lines (b) and inline (c) across the Utsira top b) An arbitrary seismic cross section across the Utsira top horizon showing the interpreted horizons and mud mounds beneath. c) A seismic cross section across the topographic high relief feature showing less relief in the interpreted Utsira base of the reservoir.

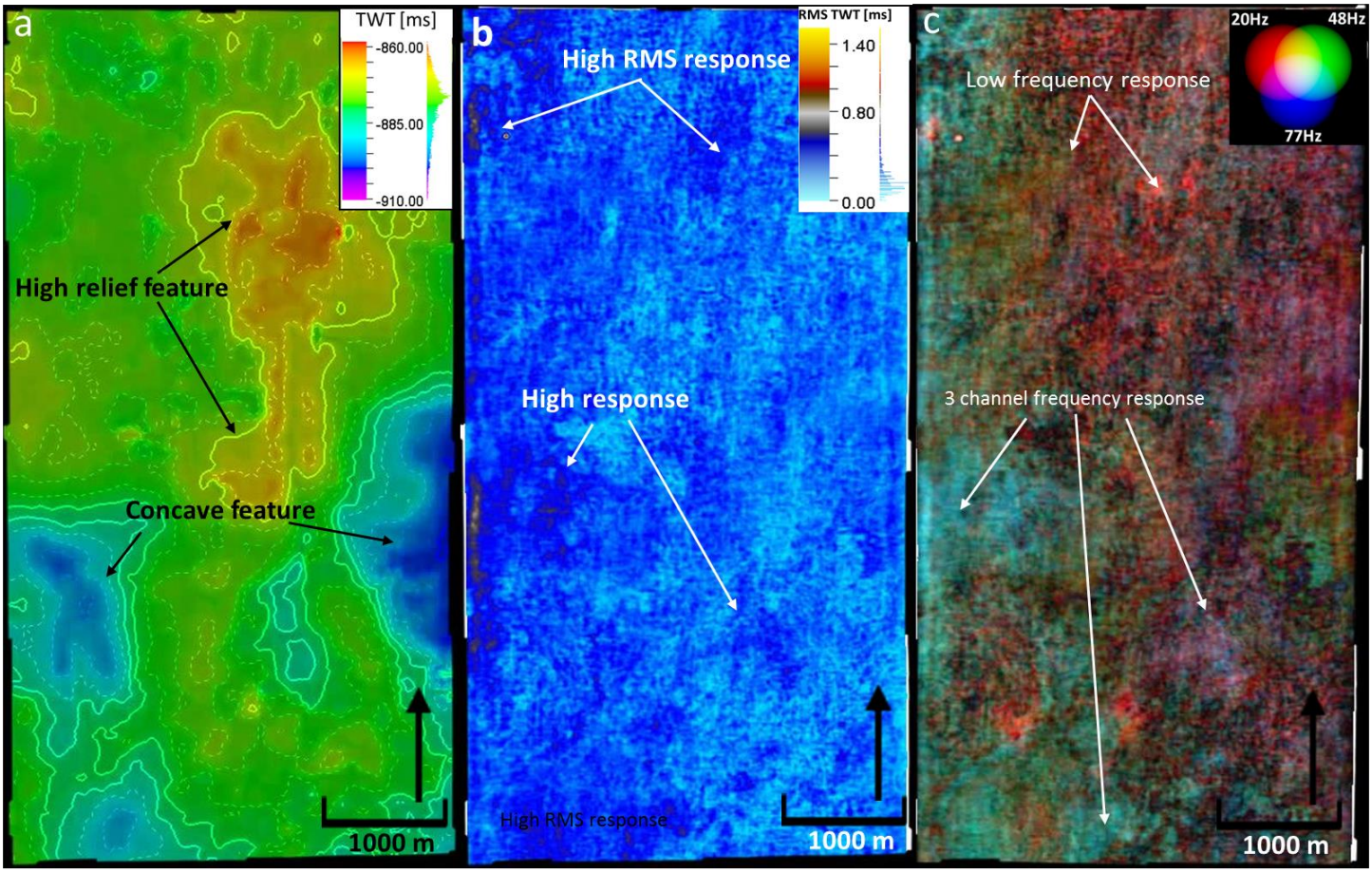

Figure 11: A 2D view attribute comparison of the Utsira top: a) Topographic map in height values of the Utsira top, b) An RMS attribute map of the Utsira top. Higher RMS response values are to the NW – W – SW of the horizon, with lower RMS values SE – E of the horizon. This shows a thinning of the horizon E to W. c) FD RGB frequency colour blend (20Hz, 48Hz, 77Hz) showing variability in the Utsira top. Uniform response from all three channels E – SE of the horizon which transition to areas with red and patches' of dark low frequency response. Intermediate response transitioning from the medium to low frequency is seen to the E and parts of the NW.

4.3 Intra Utsira Shale Units (IUTS)

The Intra Utsira Shale units are defined by the intra-reservoir seismic packages that exist between the Utsira top and Utsira base horizons. These seismic packages are interpreted as peaks on gamma ray logs and neutron density logs (figure 13). The gamma ray log peaks of the Utsira Formation in well 15/9-13 correspond to peaks in other wireline logs of other wells within a 10 km radius (Zweigel et al., 2000; Isaksen and Tonstad, 1989). These peaks represent thin shale packages with an average thickness of ca. 1.3m, computed from 5 selected wells (Zweigel et al., 2000). A total of ten IUTS were interpreted as a negative polarity trough reflector across the 3D seismic data (figure 12 and 13).

4.3.1 Seismic and Log Characteristics of the IUTS 1 to 10

Gamma ray and neutron density logs from well 15/9-13 (figure 13) show a saw tooth signature log with irregular peaks indicating a sand formation with interbeds of thin shales. The top and base of these shale layers correspond to the positive and negative reflection coefficient as seen in figure 13 (Zweigel et al., 2000). After completing a seismic well tie, the irregular gamma ray peaks corresponding to both strong and weak negative trough reflectors in the seismic data were interpreted as thin shale layers, while strong positive polarity reflectors were interpreted as sand units within the formation. The thin shale layers have a higher density and velocity than the surrounding sand in the Utsira Formation (Zweigel et al., 2000).

The seismic characteristics of the interpreted intra Utsira shale units are referred to as IUTS1 – IUTS10 (figure 12 and 13). Figure 12 shows a representative seismic section comparing the use of normal amplitude against the Instantaneous Phase and Cosine of Instantaneous Phase attributes. The use of attributes were limited to the point of continuity of the amplitude reflection within the seismic data. The characteristics of interpreted amplitude reflectors are classed into: a, Continuous – fairly continuous and b, Discontinuous – terminal amplitude reflectors which are describe below.

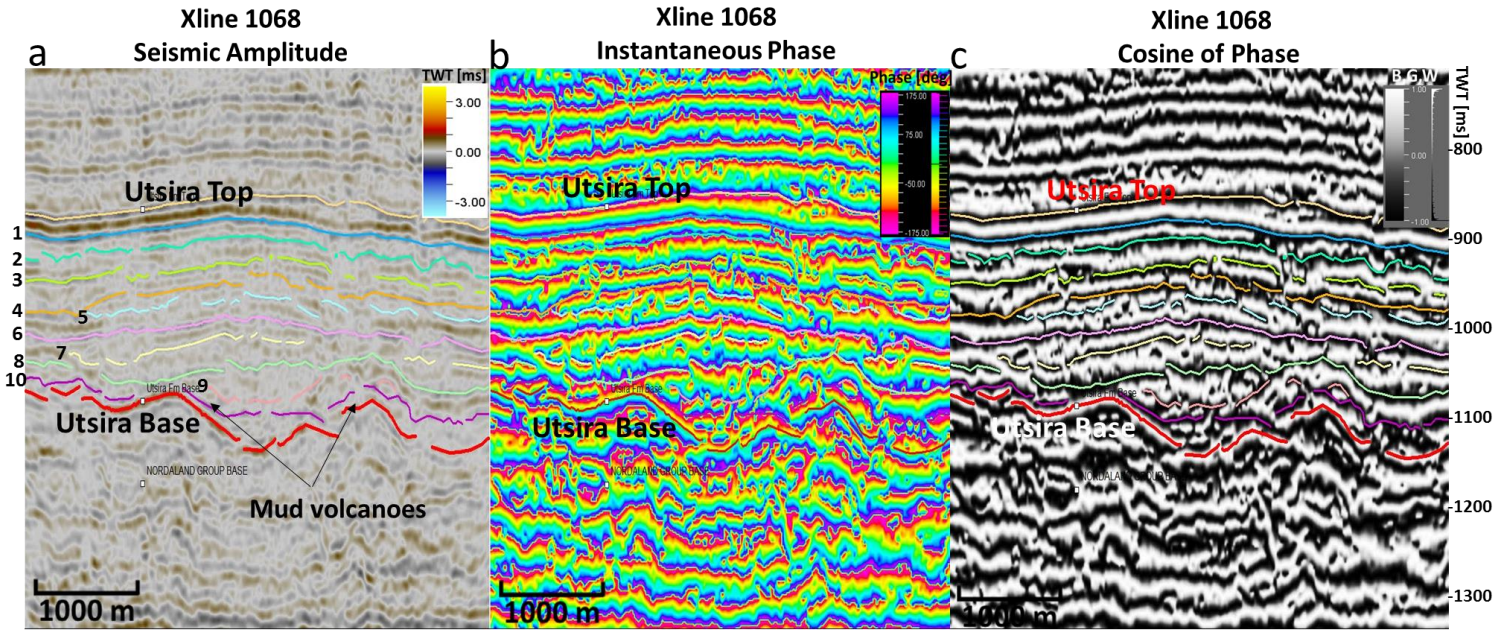

Figure 12: Seismic cross section showing the interpreted horizons across a normal amplitude and two seismic attributes. a) Cross section of a normal amplitude seismic data, crossline 1068 showing the Utsira top and base and IUTS 1 – 10. b) Cross section of an Instantaneous Phase attribute, crossline 1068 showing the Utsira top and base and the IUTS 1 – 10 horizons with a brighter reflector illumination of the seismic data. c) Cross section of Cosine of Phase attribute, crossline 1068 showing the Utsira top and base and the IUTS 1 – 10 horizons with a grey scale. Used together it is possible to interpret the thin shales and layers.

The reflection strength of the interpreted IUTS within the 3D seismic data contains information that is sensitive to absorption and scattering, and also the presence of fluids and sedimentary structures in the Utsira Formation.

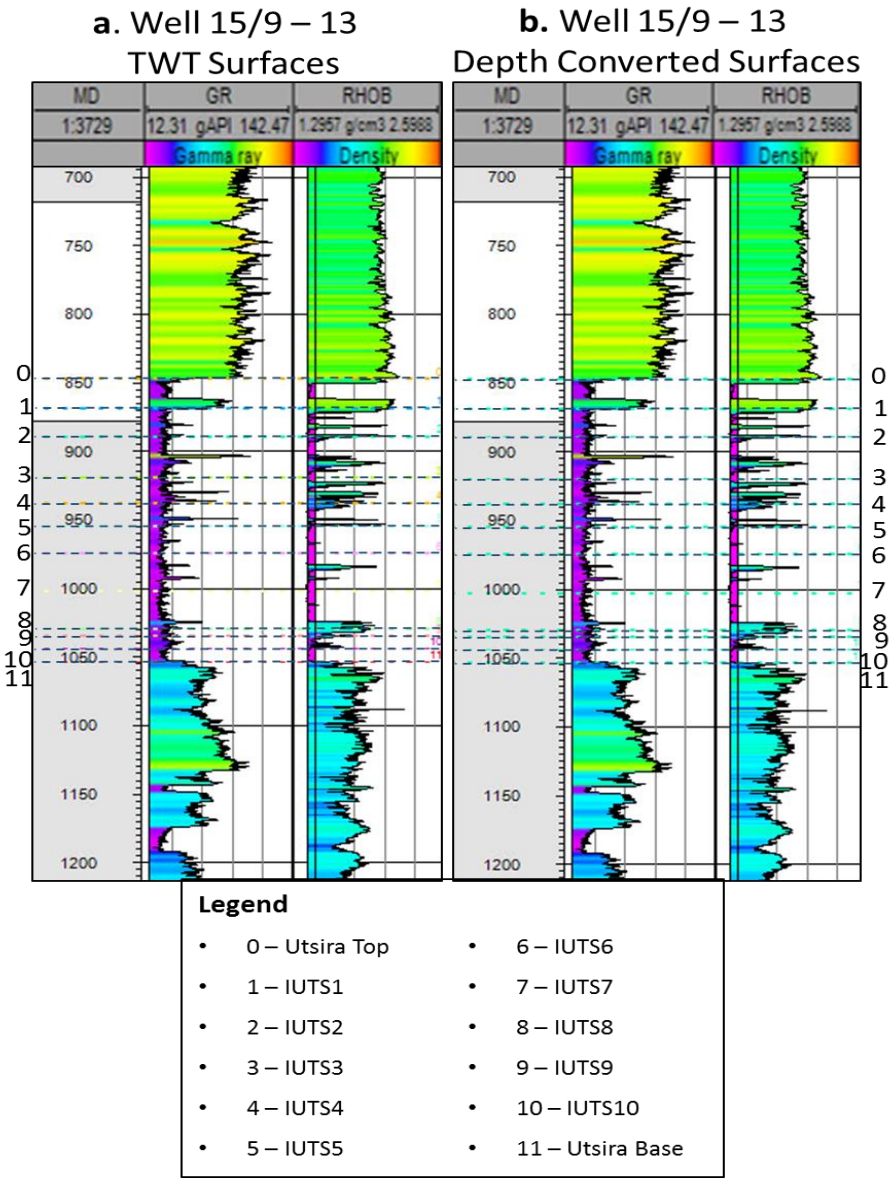

Figure 13: Well 15/9-13 showing gamma ray log and density log with check shot of the Utsira top and Utsira base, in-between are the Intra-Utsira Shales interpreted on seismic data and tied to the well. a; Interpreted time horizons shown on well 15/9-13 b; Depth converted time horizons shown on well 15/9-13. Note that there is no notable difference in the measured depth shift between the time and depth converted horizons.

The IUTS1 is identified on the gamma ray log as a very distinct peak (figure 13) and is interpreted as a shale horizon. On the 3D seismic data the IUTS1 has a distinct continuous reflector of negative polarity and similar amplitude architecture to the Utsira top. A few breaches in the rather continuous reflector were identified, these have low and chaotic vertical amplitude reflectivity and are interpreted as gas chimneys.

IUTS2, IUTS3 and IUTS4 amplitude reflectors were tied to peaks on the gamma ray and neutron density logs and have identifiable reflectors. These reflectors are interpreted as discontinuous thin shale layers, the discontinuities potentially acting as high permeability connectors between sand packages. IUTS2 and IUTS3 have reflectors that are discontinuous and phase out.

IUTS6 has no gamma ray peak response on the well logs, but has a distinct amplitude response with a fairly continuous reflector. IUTS8 was identified as a peak on the gamma ray and neutron density log that pinches out onto the top of the mounds. IUTS6 and IUTS8 are interpreted as shale layers due to their distinct amplitude reflectivity response.

The IUTS10 reflector was identified as the last peak response on the gamma ray and neutron density logs before the Utsira base. The IUTS10 is interpreted as a thin shale layer and has a reflector that simulates the reflector of the Utsira base except for areas that have been affected by uplift of mounds where the reflector either terminates or onlaps onto.

The IUTS5, IUTS7 and IUTS9 have small gamma ray log peaks (figure 13) and on the 3D seismic, the reflectors are frequently discontinuous. IUTS5, 7 and 9 are seen to pinch out to the east and west of the study area. IUTS5 forms a toplap onto IUTS4 while IUTS7 onlaps onto IUTS8 and IUTS9 onlaps onto IUTS10. IUTS7 is seen pinching out onto underlying horizons. IUTS9 occasionally pinches out onto the relief mounds.

4.3.2 IUTS Horizon – Surface Geometry

The interpretation of IUTS 1 to 10 reveals a conformable horizon sequence with a geometry influenced by the mound relief features at the Utsira base. Figure 14a shows a 3D view of the interpreted horizons stacked together. In the upper units, IUTS1 – IUTS7 show thinning of the Utsira Formation to the south

(figure 14b – d and table 1). IUTS1 is the thickest of the IUTS packages and has a relief feature that extends for ca. 3 km with a width ranging from 1 km to 2 km and heights ranging from ca. 5 m to 20 m (figure 15a). The same relief and concave features are apparent across the interpreted IUTS packages. The height value normal amplitude of IUTS 4 reveals a subtle relief structure at the north east and south east of the surface, with a height range of ~ 20 m across the horizon, and concave features ranging in depth of about ~ 10 m (figure 15d). Towards the base of the Formation IUTS 8 - IUTS10 the topography of the shale units are affected by intrusion and uplift of the mounds (figure 14d-e).

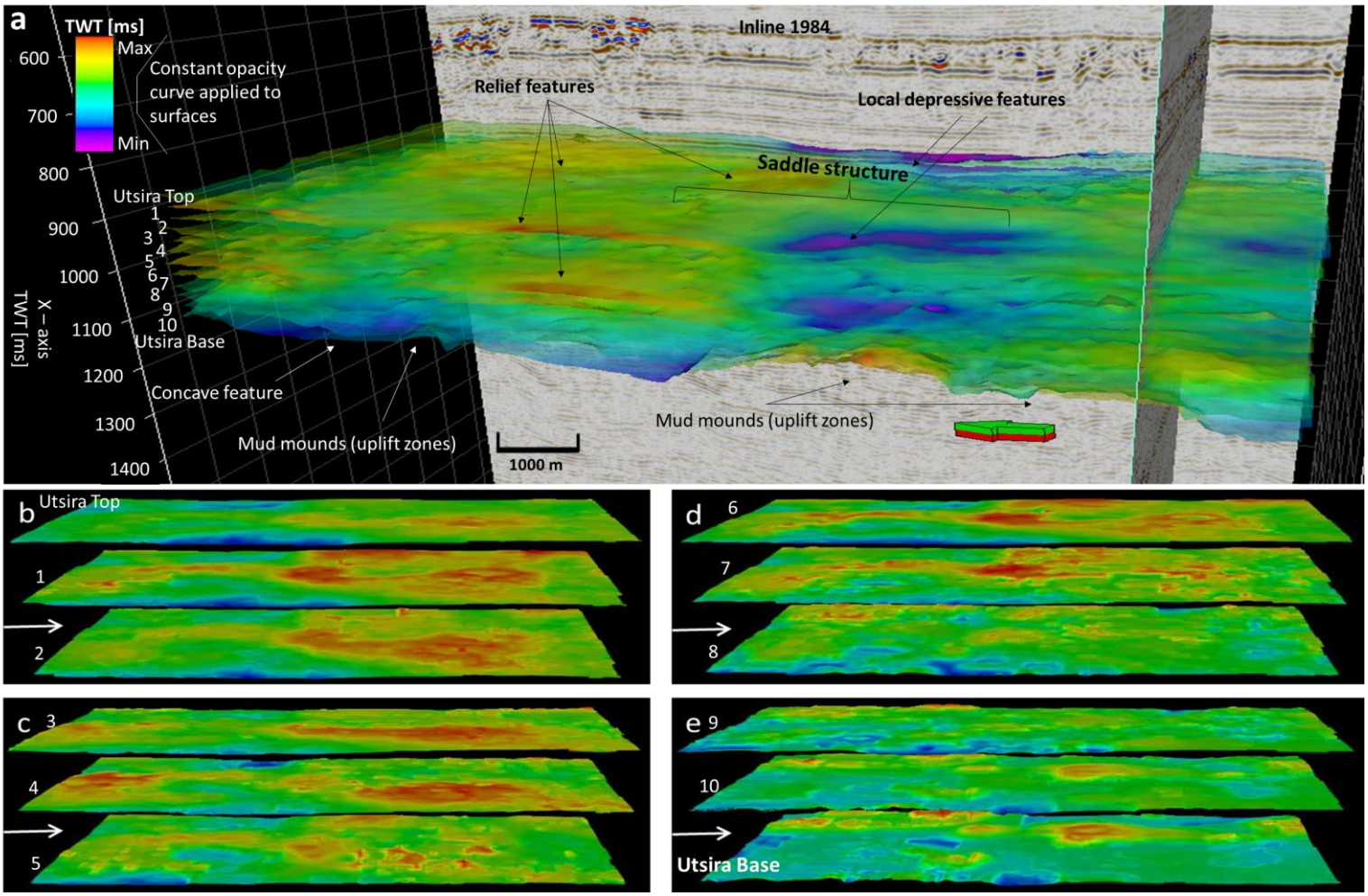

Figure 14: 3D seismic data of the Sleipner field study area and the interpreted horizons. a) 3D view of the mapped horizons in height values; Utsira top and bottom and IUTS1 – 10. Refer to figure 1b and 8b for location map. Transparency has been applied to the horizons in other to reveal the stratigraphic relationship of the highest and lowest height values thus revealing a saddle structure. b) Mapped horizons from the Utsira top to IUTS 2, sheared to reveal the topography of the horizons. c) Mapped horizons from the IUTS3 – IUTS5, sheared to reveal the topography of the horizons. d) Mapped horizons from the IUTS6 – IUTS8, sheared to reveal the topography

of the horizons. e) Mapped horizons from the IUTS9 – Utsira top, sheared to reveal the topography of the horizons.

4.3.3 Comparison of IUTS attribute responses

Two IUTS horizons are presented in figure 15 to show the tuning and frequency response variability of IUTS 1-10. IUTS1 has a higher amplitude RMS response across the surface and a responsive RGB frequency blend (figure 15b, c), which reveals details interpreted to be related to the variability response of the thickness and petrophysical properties of the horizon.

The RMS response of IUTS4 is fairly uniform showing low amplitudes, with a few high amplitude spots. The RGB frequency blend shows greater variation with a low frequency response (red) transitioning to dark grey and dark red areas to high frequency response (dark blue) indicating areas of seismic discontinuity.

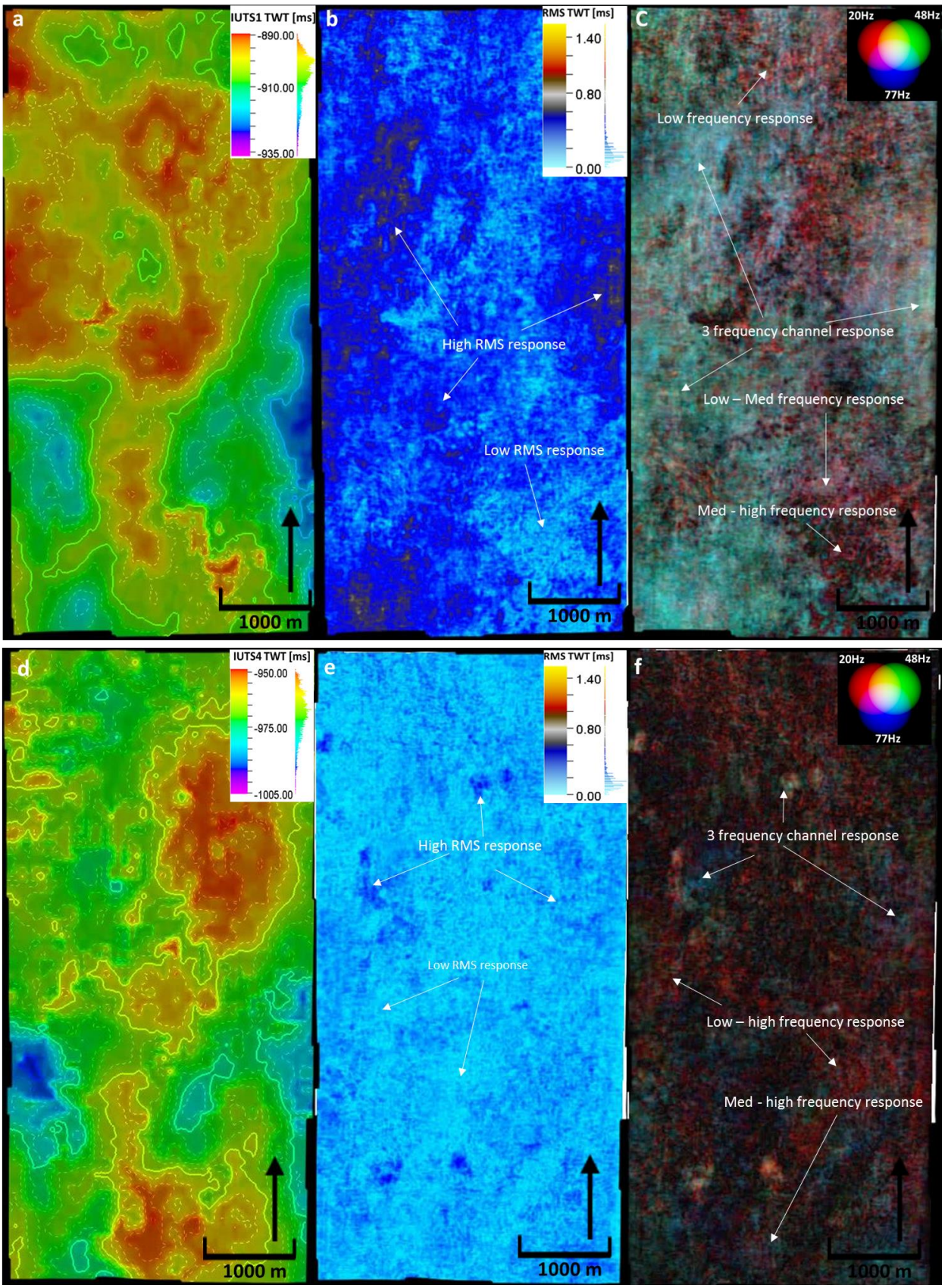

Figure 15: A 2D view attribute comparison of the IUTS1 and IUTS4: a) Topographic map in height values of the IUTS1, b) An RMS attribute map of the IUTS1. High amplitude values are due to thin beds above seismic resolution, transitioning to low amplitude value across the area with relatively high elevations central - SE c)

Frequency Decomposition RGB frequency colour blend (20Hz, 48Hz, 77Hz) showing variability in the IUTS1. Uniform response from all three RGB channels displayed in white-grey colour while red indicates thick beds, and dark colours indicate low response from channels, due to low tuning thickness and facies change across the horizon. d) Topographic map in height values of the IUTS4, e) An RMS attribute map of the IUTS4. A uniform RMS low value across the horizon, indicative of thin beds below seismic resolution and f) FD RGB frequency colour blend (20Hz, 48Hz, 77Hz) showing variability in the IUTS4. Dark red to dark colours, indicate weak frequency response that transitions to areas with medium frequency response.

Figure 16 shows 4 mapped horizons in TWT, compared against the depth converted maps and RMS attribute map of the same area. With a single well used for quality control and an interval velocity of 2109.59 $^{ms-1}$ and 2132.78 $^{ms-1}$ (Utsira top and Utsira base respectively), the depth converted horizons achieved a close match between well observations (figure 13b) and depth converted seismic horizons (figure 16).

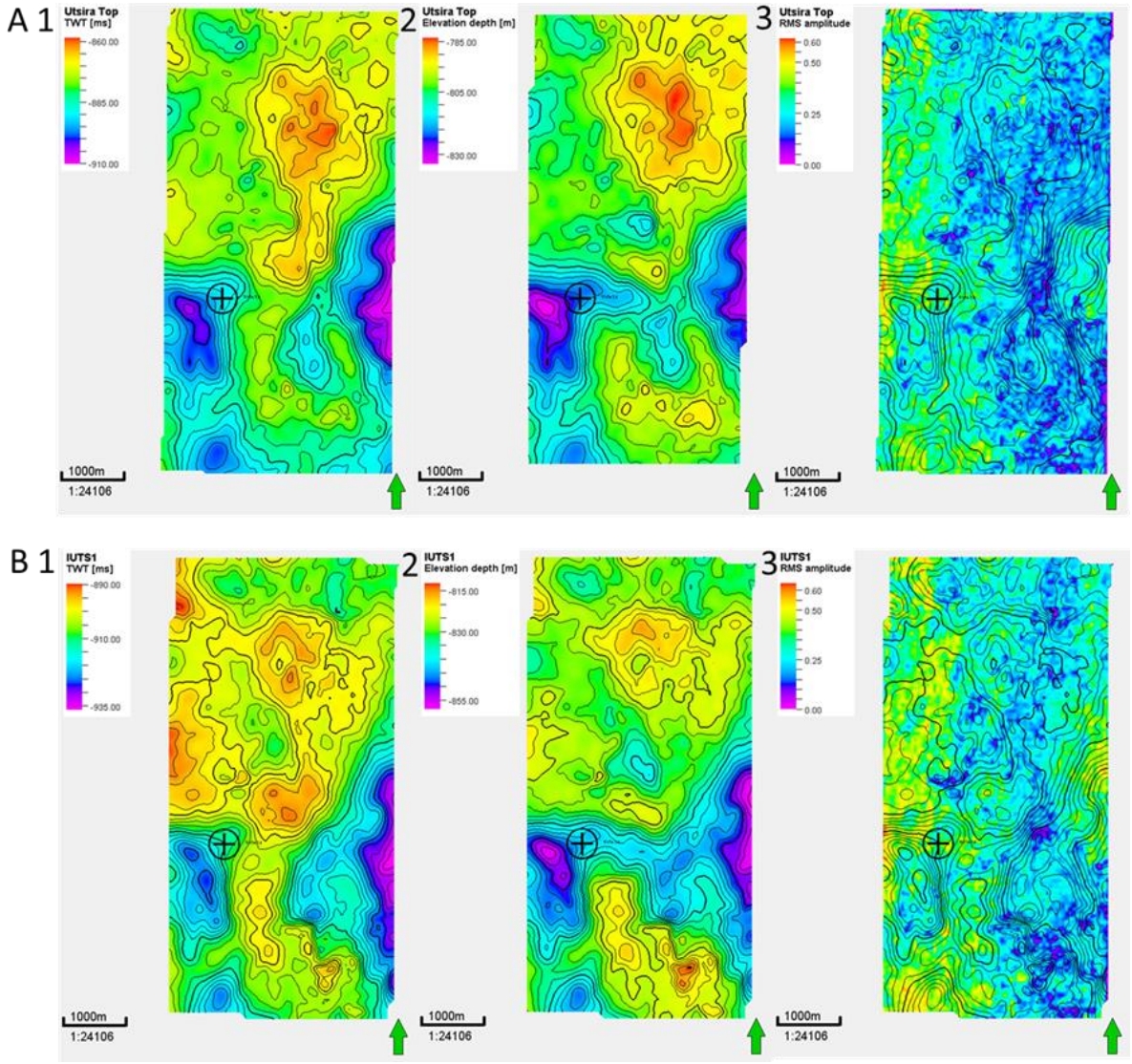

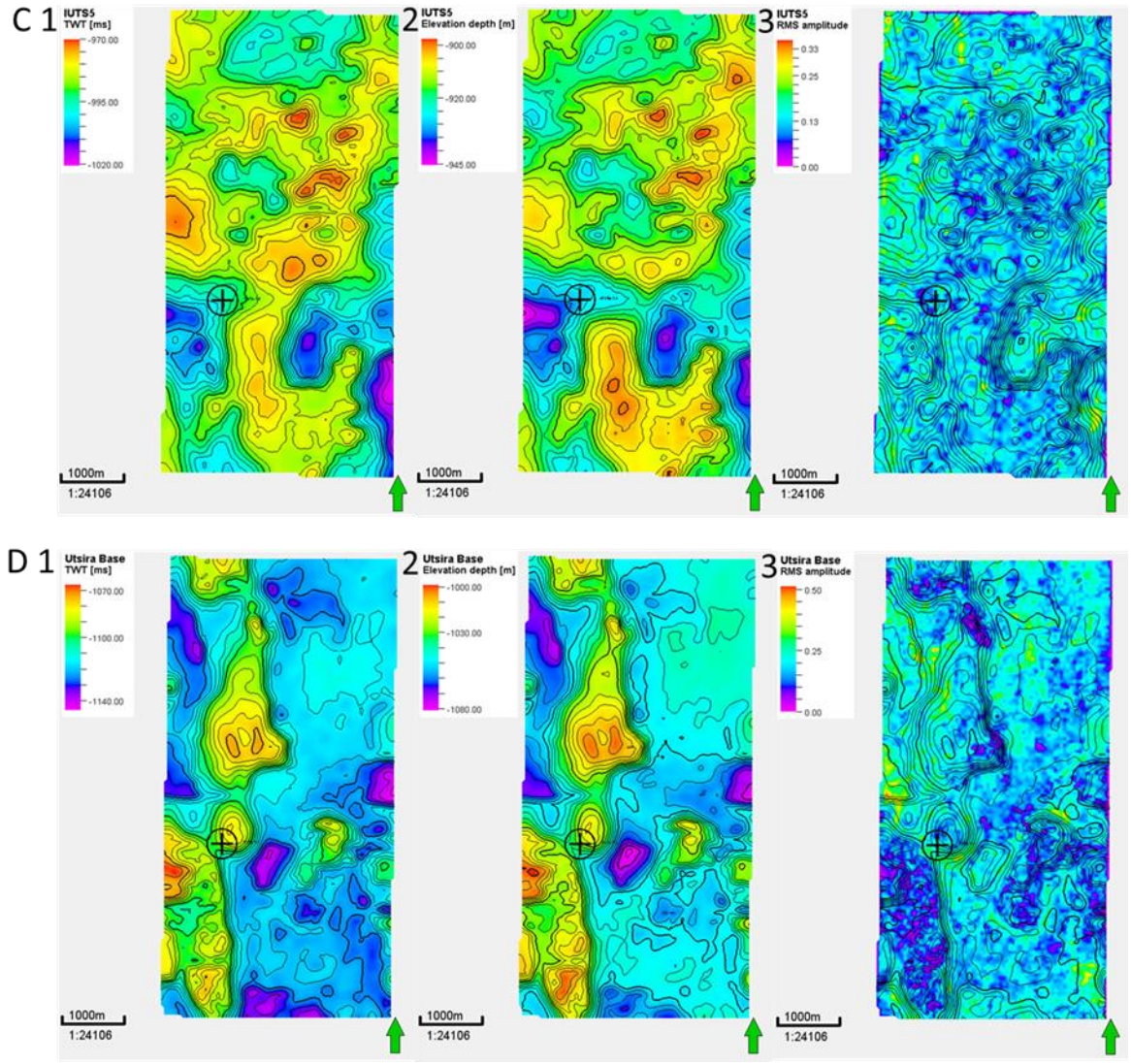

Figure 16: TWT [ms] seismic and depth [m] converted surfaces of the Utsira Formation. A: Utsira top surface map displayed as 1) TWT map, 2) Depth converted map, 3) RMS attribute of the TWT seismic map. B: IUTS1 surface map displayed as 1) TWT map, 2) Depth converted map, 3) RMS attribute of the TWT seismic map. C: IUTS5 surface map displayed as 1) TWT map, 2) Depth converted map, 3) RMS attribute of the TWT seismic map, 4) Utsira base surface map displayed as 1) TWT map, 2) Depth converted map, 3) RMS attribute of the TWT seismic map

4.4 Identification of gas chimneys - fluid flow features

Within the study area, stacked high seismic amplitude anomalies are identified, these are mainly interpreted as gas chimneys within the reservoir. These gas chimneys are often defined by pockmarks in map view with the high seismic amplitude anomalies seen in cross section at their vertical termination zone (figure 17), due to accumulation of gas in the Pliocene strata units. Multi-attribute analysis is used to delineate the form and occurrence of these gas chimneys as high diapiric seismic amplitude that can be vertically traced (figure 17f, 18).

High seismic amplitude anomalies or bright spots are predominantly identified at depths of -620 ms – -750 ms (-550 m – -670 m) across the interfaces of the Pliocene units (figure 17). High seismic amplitude anomalies may occur due to the presence of biodegraded or thermogenic hydrocarbons (i.e carbonate diagenetic cementation) or the accumulation of shallow gas, originating through mud diapirism from the mud mounds beneath the Utsira base (Heggland, 1997). The anomalies have a NE-SW trend and are seismically characterised by a hard reflection of a positive red to yellow colour contrast. The anomalies opacity colour (figure 18a and b) are indicative of a transition zone from low acoustic impedance such as a gas charged sandstone to a high acoustic impedance such as shale, or a carbonate cemented surface. Anomalous rich zones are also seen on the clinoform geometries that downlap from a prograding Pliocene sequence (figure 17b). According to Heggland (1997) the distribution of mud volcanoes across the study area correlates with the high amplitude anomalies in the Pliocene units. Identification of the potential gas pathways associated with these high amplitude anomalies is key to understanding if chimneys exist within the formation.

Chimneys can be seismically identified as vertical curvilinear features seen across the Nordland Group within the 3D seismic cube and can be traced from the mounds at the Utsira base to the Pliocene top where they are seen to terminate with a high seismic amplitude anomaly. The gas chimneys and their pattern of occurrence are described in Løseth et al., (2009) and Løseth et al., (2011). Results of the multi-attribute analysis identified seismic anomalies and allowed the visualisation of gas chimneys, defined by curvilinear features occurring above the mound relief features MRF1 – 6 (figure 17 and 18). Figure 17 shows a comparison of a normal amplitude and noise cancelled data of the same seismic section, comparing the use of individual chaos and envelope attribute to the multi-attribute that combines both the chaos and the envelope attributes.

In figure 17, the square box highlights a vertical wipe out zone. This wipe-out zone cross-cuts through the Utsira top to the top Pliocene units, where high amplitude anomalies are interpreted as trapped gas (Heggland, 1997). The features can be better distinguished after multi-attribute analysis. The gas chimney is seen as a vertical curvilinear feature with high amplitude anomalies occurring at its flanks

and terminating against the amplitude anomaly (figure 17 and 18). Our interpretation is that the curvilinear features act as gas chimneys or feeder pipe structures across the formation. The patchy appearance of gas gives an irregular distribution of low velocity zones within the seismic data that in turn deteriorates the seismic imaging of areas beneath such zones (figure 18b). The chimneys vary from sub-vertical to vertical, when viewed in cross section (figure 17, 18). The boundaries between these features and the surrounding stratigraphic reflections is best imaged using multi-attribute analysis where the outside adjoining stratigraphic reflection reveals a dimmed or consistent reflection (due to high frequency) or a bright stratigraphic continuity.

There are three zones that are identified in relation to gas chimneys (figure 18) described according to Løseth et al., (2009): a) The root zone, b) the leakage zone feature and c) the leakage top zone. Six possible root zones have been identified in this study and are referred to as the mound relief feature labelled MRF1 – MRF6 (figure 18). The leakage zone is the rock volume zone of the reservoir that is influenced by vertical migrating fluids. Note that not all gas chimneys impact the rock properties sufficiently enough to give a high seismic expression in the normal amplitude data (figure 18d). In figure 18, the gas chimneys are seen to terminate at high seismic anomalies. This is the leakage top zone identified in the Pliocene units. It is the upper zone of termination where the chimneys either end or their continuity is dimmed by the seismic anomaly due to accumulation of gas.

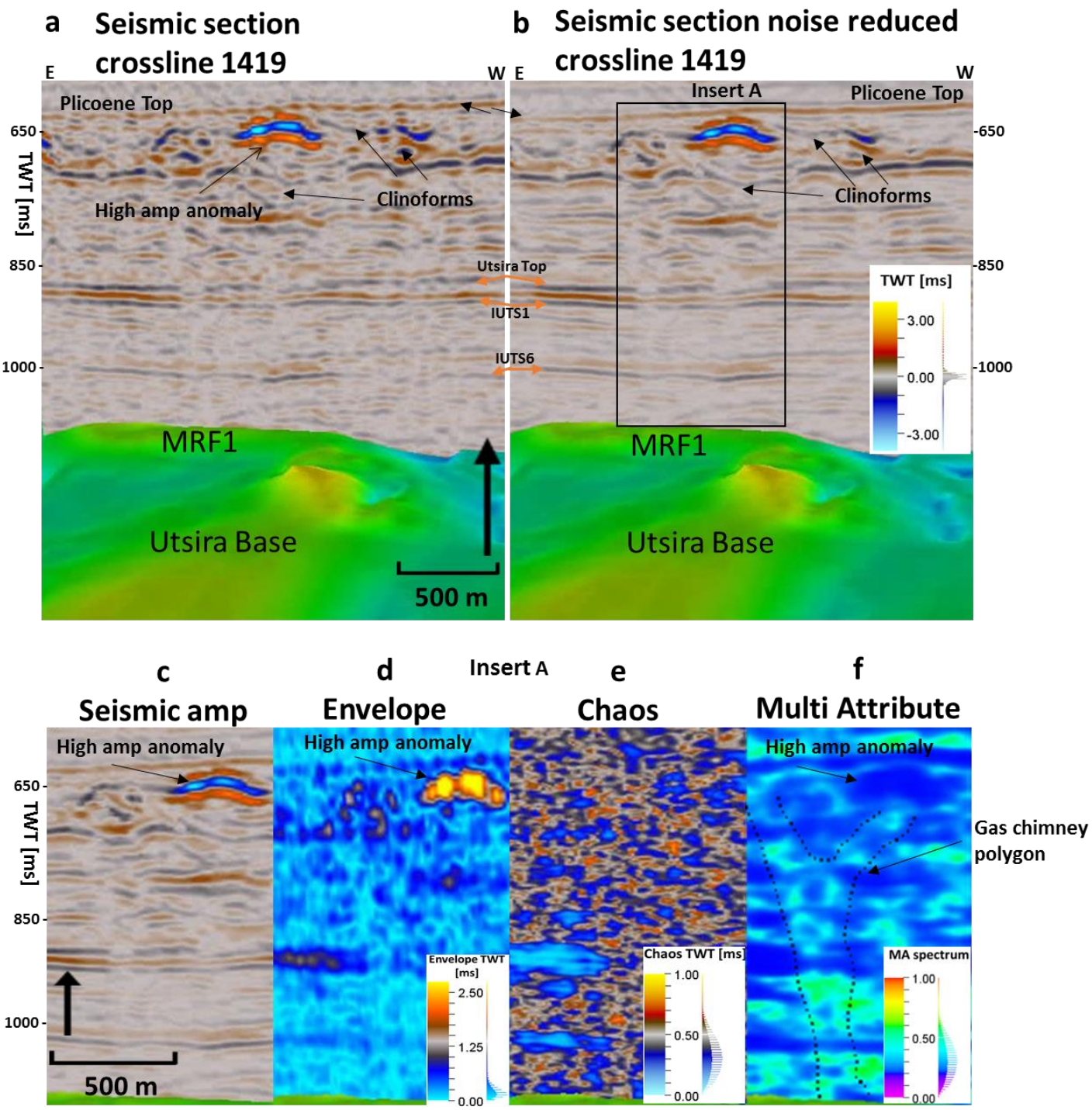

Figure 17: 3D Seismic cross section crossline 1419 above a mud mound in the Utsira base comparing attributes. a) 3D cross section crossline 1419 of the normal seismic data showing mud mound (MRF1) and the high amplitude anomaly. b) 3D cross section crossline 1419 of a noise reduced seismic data, notice the reduction in jitters across the seismic section. Insert A, a rectangular polygon around area of interest. c) Insert A seismic cross section of noise reduced data, d: Insert A seismic cross section of an envelope attribute highlighting the high seismic anomaly. e) Insert A seismic cross section of a chaos attribute highlighting the chaotic pattern within and, f) Insert A seismic cross section of a diaper attribute which combines the use of chaos and envelope to generate a more coherent attribute with the potential to reveal gas chimneys.

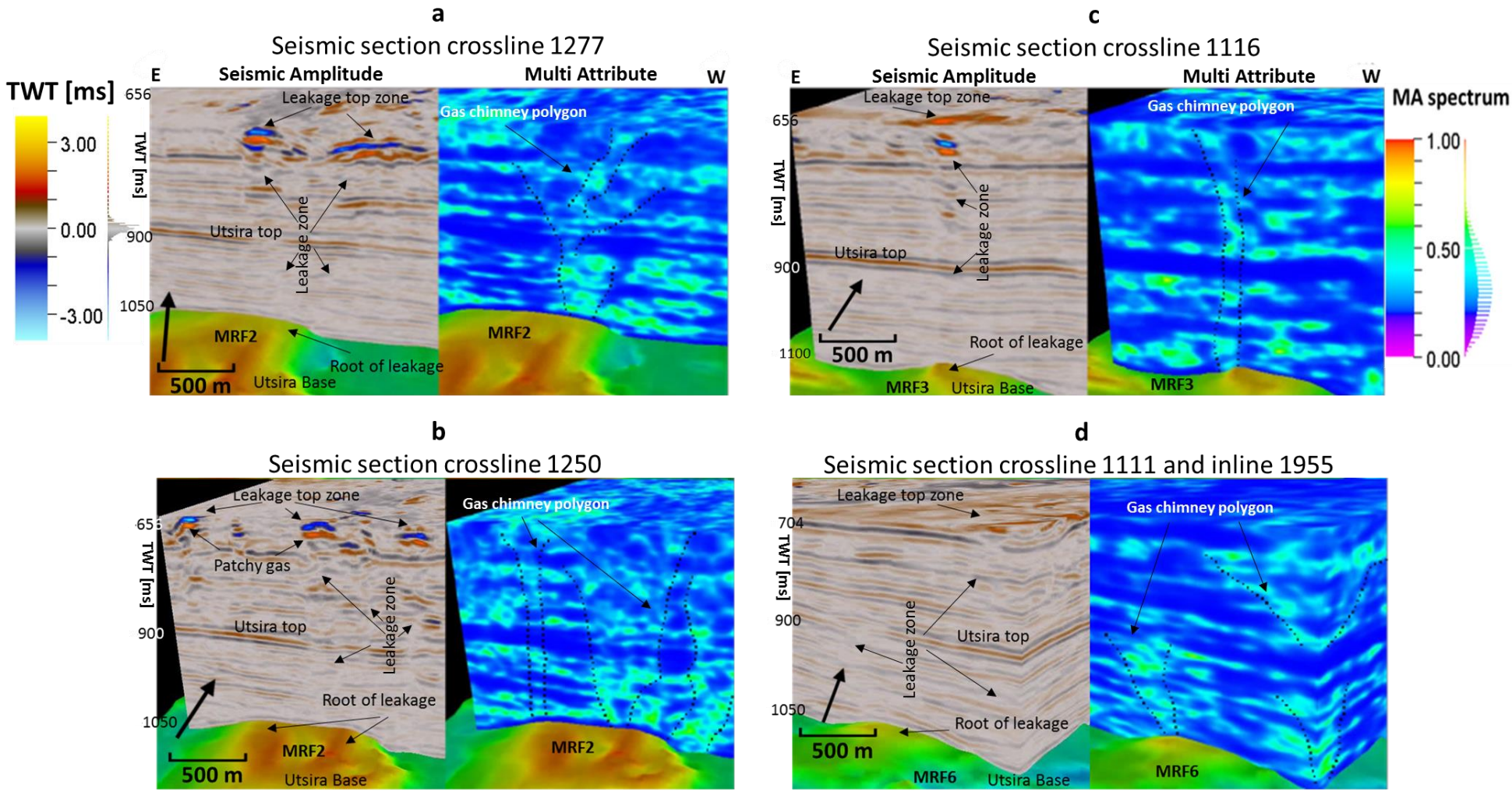

Figure 18: 3D Seismic cross section of the study area above 3 mud mounds in the Utsira base showing a normal amplitude compared against the multi-attribute to better reveal the gas chimneys across the data. a) Seismic section crossline 1277 above MRF2 showing the root of leakage, leakage zone and leakage top zone - high amplitude anomalies in the Pliocene units. The multi-attribute has highlighted the gas chimney as indicated in dotted polygon lines. b) Seismic section crossline 1250 above MRF2 ~68meters apart from fig 18a, showing the root leakage, leakage zone and high amplitude zone – patchy distribution of gas in the Pliocene units. The multi-attribute has highlighted the same gas chimney feature in dotted polygon lines with a wider spread and more zones of leakages. c) Seismic section crossline 1116 above MRF3 showing the root of leakage, leakage zone and above in the Pliocene units high amplitude anomalies – leakage top zone. The multi-attribute has highlighted the gas chimney features as indicated in dotted polygon lines. d) Seismic section crossline 1111 and inline 1955 above MRF6 showing the root of leakage, leakage zone and leakage top zone – high amplitude anomalies in the Pliocene units. The multi-attribute has highlighted the gas chimney features in two directions as indicated in dotted polygon lines thus indicating a semi – circular tabular orientation.

5.0 Discussion

In order to determine the detailed reservoirs architecture, we have carefully interpreted the stratigraphy outlined by the amplitude, phase and frequency content of the seismic data. The use of the Instantaneous Phase and Cosine of Instantaneous Phase to aid the interpretation of discontinuous seismic reflectors from normalised amplitude is instrumental to understanding the topography, and petrophysical variability within the reservoir. The observed variability can be used to constrain the possible flow of hydrocarbons, fluids and of relevance to this case injected CO_2.

The results of the combined seismic attribute analysis have allowed us to build a clear 3D picture of reservoir heterogeneity for the Sleipner field. This heterogeneity is summarised in a schematic 2D cross section through the reservoir (figure 19).

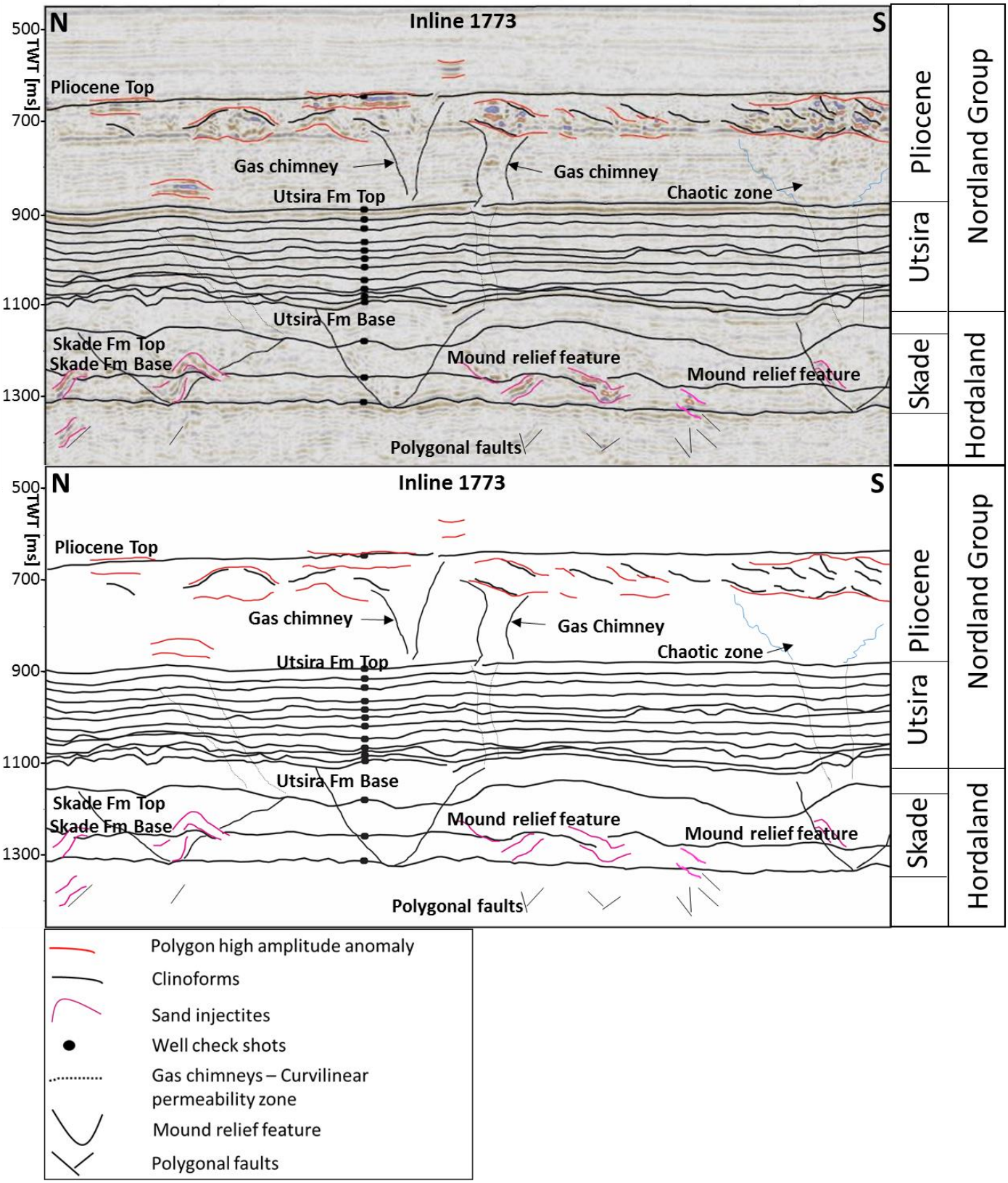

Figure 19: Schematic architecture diagram of a seismic cross section inline 1773 showing the interpreted horizons and structures of the study area. Schematic architecture illustrates the sedimentary features at play within a reservoir. The mound relief feature cross cuts the stratigraphic horizons of the Skade Fm.

Figure 19 is a representative seismic cross section of the architecture of the Utsira Formation in the Sleipner Field area. The cross section shows the existence and extent of mound relief features at the base of the Utsira Formation (Hordaland Group) with the presence of minor scale sand injectites and polygonal faulting at the flanks of the mud mounds as described in Wild and Briedis, (2010) and Satur and Hurst, (2007). The architecture of the Utsira Sand shows lines of interpreted thin interbedded muds with polygons around areas of low chaotic zones interpreted as gas chimneys. These features permit the flow of reservoir fluids and gases across the stratigraphic layers till they terminate at impermeable sedimentary layers. High amplitude anomalies are visualised at the top Pliocene units (figure 19), interpreted as gas trapped against clinoforms and impermeable sedimentary layers.

5.1 Implications for CO_2 storage capacity

The interpreted units represented in depth values can be used to calculate the difference in thickness between each interpreted unit. The total pore volume of the Utsira Sand across the two depocentres has been estimated to be roughly 5.5 x 10^{11} m^3 assuming an average porosity value of 30% as calculated by Chadwick et al., (2000).

Within the 3D seismic survey used the thickness of the Utsira Formation ranges from 180 m to 200 m, local depth variations are due to the presence of mud mounds at the Utsira base. Holloway et al., (2000) calculated the Utsira Sand Formation total spore space by multiplying the Utsira Sand Isopachs by the sand porosity and proportion of clean sand. We however calculated the total volume of the Utsira Sand in the survey area based on a conservative summed average difference in depth thickness of the sand between the Interpreted thin shale horizons (table 1).

The total calculated volume is 3.51 x 10^9 m^3. Assuming an average porosity of 30 % across the Utsira Sand the total average pore volume is 1.05 x 10^9 m^3. Our calculation predicts a significantly reduced volume for CO_2 storage in the Utsira Formation of the Sleipner field then that of Chadwick et al., (2000).

In the case of CO_2 sequestration, storage directives require that the CO_2 be sequestered in a structurally closed feature. In this case the Utsira cap rock acts as a seal above the Formation (Chadwick et al., 2004). The Utsira Formation intra reservoir shales range from continuous to discontinuous and can be regarded as impermeable to semi permeable shales allowing the flow of fluids and gases to the Utsira top. The interpreted IUTS horizons show a general southward dip with low domal and anticlinal relief features N-S and concave features (figure 14 and 16). This suggests that on a local scale, it can be predicted that reservoir fluids, injected CO_2 and or hydrocarbons will follow the local maximum topographic gradient of the intra-reservoir units. The geometries of the IUTS units, e.g. relief and concave features could act as stratigraphic traps for CO_2 (figure 14a). Pressure differences within reservoirs will affect flow pathways. Based on the frequency response to tuning thickness, layer stacking and variability in rock impedance across each unit, we predict that pressure differences will likely exist within the reservoir during CO_2 injection. Thus the understanding of the geometry of the intra-reservoir shales presented here is of importance for injection planning and migration prediction, as subtle differences between barrier horizons can have a decisive influence on flow pathways and reservoir efficiency (Zweigel et al., 2001). Contrary to past research (Chadwick et al., 2000; Zweigel et al., 2000 Zweigel et al., 2004; Holloway et al., 2000; Chadwick and Noy, 2010) that have predicted CO_2 plume geometry within the reservoir, based on available 4D data and mapped the Utsira top and the sand wedge, we have used the initial 3D seismic survey to predict flow paths. The efficacy of our mapping will be tested against the available 4D seismic data of the study area that shows the distribution of the CO_2 plume within the reservoir in future work.

5.2 Gas chimneys - implications for fluid flow

Prior to the sequestration of CO_2 in the Utsira Formation, high amplitude seismic anomalies and gas chimneys were identified in the Pliocene units overlying the Utsira Formation (Heggland, 1997). The form and occurrence of these high amplitude anomalies are further described in Loseth et al., (2003); Cartwright et al., (2003); Jackson and Stoddart, (2005).

The assumption is that these gas chimneys are linked to the mud diapirs formed during the Late Oligocene to early Miocene. These mud diapirs collapsed as the Utsira Sands where deposited over them in the Early to Mid-Miocene, forcing the expulsion of fluids and gases through the Utsira Sand. The fluids remaining in the Utsira Formation then migrated upwards to the Pliocene units where the fluids accumulated.

An immediate question is do the gas chimneys undermine the integrity of the Utsira Sand Formation as a favourable repository for CO_2? As the gas chimneys can be traced from the Utsira base to the Pliocene top units. Or could it be that the high seismic amplitude anomalies at the Pliocene Units are resulting in a possible velocity push down effect (figure 18c)? It is rather difficult to map these gas chimneys in the seismic data due to the low amplitude of their seismic facies with regards to the surrounding amplitude (Eduardo and Matos, 2013). However, the use of the multi-attribute has facilitated the identification of the spatial distribution of these gas chimneys across the data.

If the gas chimneys act as high permeability pathways following the injection of CO_2 into the formation leakage past the Utsira caprock may occur. It is also worth noting that, these preferential pathways may also exist in the formation as faults or through a network of interconnecting fractures and fissures (Harrington and Horseman, 1999), below the resolution of current seismic imaging. The injection of CO_2 mixing with saline water forms a weak acid that could possibly aid in the initiation and reactivation of fractures (Shukla et al., 2010) and hence fluid flow paths.

The application of mapping thin beds and identifying pre-existing gas chimneys can be adapted to suit reservoir needs and is applicable not only in the sequestration of CO_2 but also in monitoring and predicting flow of hydrocarbons, reservoir fluids and hydraulic fracturing for unconventional hydrocarbons.

6.0 Conclusion

The interpretation of the Utsira base and top conforms to the regional description of the interpretation of the Sleipner field by Holloway et al., (2000) ; Løseth et al., (2009) and Zweigel et al.,

(2004). The use of complex seismic trace attribute analysis enhanced conventional seismic interpretation of thin shale layers and aided the identification of gas chimneys. The interpretation results define the internal architecture of the Sleipner reservoir, revealing 10 intra Utsira shale layers with topographic relief features trending NE – SW within the Utsira Formation. The interpreted horizons reveal variability as a response to changes in tuning thickness, rock acoustic impedance and facies change when analysed using the RMS seismic attribute and Frequency Decomposition, aiding interpretation. The thin shale layers are interpreted as acting as impermeable to semi-permeable stratigraphic 'trapping' layers within the Utsira Sand. High permeability fluid flow structures, gas chimneys, are best visualised and identified using multi-attribute analysis; their identification can help predict flow paths between sand layers separated by thin shale layers. Seismic interpretation of thin shale layers, with the use of seismic attributes and spectral analysis, in a reservoir outlines the internal architecture of a formation. Such detailed interpretation can be used to conservatively calculate available pore volume and predict the future distribution and storage potential of CO_2, or other fluids. Further, the identification of pre-existing high permeability chimney structures; that could be reactivated by the injection of CO_2, or other fluids, enable risk assessments for storage stability and the identification of potential high permeability pathways to be made.

Acknowledgments

The seismic interpretation and image processing was carried out in the SeisLab facility at the University of Aberdeen (sponsored by BG BP and Chevron). Seismic imaging analysis was performed using GeoTeric (ffA), and analysis of seismic amplitudes was performed in Petrel 2015 (Schlumberger). We would like to thank the NDDC (RG11766-10) for funding this research and Statoil for the release of the Sleipner field seismic dataset utilized in this research paper and also Anne-Kari Furre and her colleagues for their assistance. We also thank the editor, Alejandro Escalona and the two anonymous reviewers for their constructive and in depth comments that improved the paper.

References

Ambrose,W.A., Lakshminarasimhan, S., Holtz, M.H., Nú~nez-L_opez, V., Hovorka, S.D., Duncan, I., 2008. Geologic factors controlling CO_2 storage capacity and permanence: case studies based on experience with heterogeneity in oil and gas reservoirs applied to CO_2 storage. Environ. Geol. 54, 1619e1633. http://dx.doi.org/10.1007/s00254-007-0940-2.

Arts, R., Eiken, O., Chadwick, A., 2004a. Monitoring of CO_2 injected at Sleipner using time-lapse seismic data. Energy I 347-352.

Arts, R., Eiken, O., Chadwick, A., Zweigel, P., van der Meer, B., Kirby, G., 2004b. Seismic monitoring at the Sleipner underground CO_2 storage site (North Sea). Geol. Soc. Lond. Spec. Publ. 233, 181-191. http://dx.doi.org/10.1144/GSL.SP.2004.233.01.12.

Arts, R., Chadwick, A., Eiken, O., Thibeau, S., Nooner, S., 2008. Ten years' experience of monitoring CO_2 injection in the Utsira Sand at the Sleipner. Offshore Nor. 26,65-72.

Avseth, P., Mukerji, T., Mavko, G., 2010. Quantitative Seismic Interpretation. Cambridge University Press, Cambridge. http://dx.doi.org/10.1029/2003JD004173.Aires.

Baker, R.O., Yarranton, H.W., Jensen, J.L., 2015. The Practice of Reservoir Characterization, Practical Reservoir Engineering and Characterization. http://dx.doi.org/10.1016/B978-0-12-801811-8.00011-0.

Brown, A.R., 2004. Interpretation of 3-D Seismic Data, 6th ed., vol. 42. AAPG Memoir. 541 p.

Cartwright, J.A., 1994. Episodic basin-wide fluid expulsion from geopressured shale sequences in the North Sea basin. Geology 22, 447-450. http://dx.doi.org/10.1130/0091-7613(1994)022<0447:ebwfef>2.3.co;2.

Cartwright, J., James, D., Bolton, A., 2003. The genesis of polygonal fault systems: a review. Geol. Soc. Lond. Spec. Publ. 216, 223-243. http://dx.doi.org/10.1144/GSL.SP.2003.216.01.15.

Chadwick, R.A., Eiken, O., 2013. Offshore CO_2 Storage: Sleipner Natural Gas Field beneath the North Sea, Geological Storage of Carbon Dioxide (CO_2): Geoscience, Technologies, Environmental Aspects and Legal Frameworks. Woodhead Publishing. http://dx.doi.org/10.1533/9780857097279.3.227.

Chadwick, R.A., Noy, D.J., 2010. History-matching flow simulations and time-lapse seismic

data from the Sleipner CO_2 plume History-matching flow simulations and time-lapse seismic data from the Sleipner CO_2 plume. In: Petroleum Geology Conference Series. http://dx.doi.org/10.1144/0071171.

Chadwick, R., Holloway, S., Kirby, G. A., Gregersen, U., Johannessen, P.N., 2000. The Utsira Sand, Central North Sea - an assessment of its potential for regional CO_2 disposal. … 5th Int.

Chadwick, R., Zweigel, P., Gregersen, U., 2002. Geological characterization of CO_2 storage sites: Lessons from Sleipner, northern North Sea. … (GHGT-6), J. Gale Y. … I, 321-326.

Chadwick, R., Zweigel, P., Gregersen, U., Kirby, G., Holloway, S., Johannessen, P.,2004. Geological reservoir characterization of a CO_2 storage site: the Utsira Sand, Sleipner, northern North Sea. Energy 29, 1371-1381. http://dx.doi.org/ 10.1016/j.energy.2004.03.071.

Chadwick, A., Arts, R., Eiken, O., Williamson, P., Williams, G., 2008. Geophysical Monitoring of the CO_2 Plume at Sleipner North Sea: Vasa. Retrieved from: http://medcontent.metapress.com/index/A65RM03P4874243N.pdf.

Chadwick, R.A., Marchant, B.P., Williams, G.A., 2014. CO_2 storage monitoring: leakage detection and measurement in subsurface volumes from 3D seismic data at Sleipner. Energy Procedia 63, 4224-4239. http://dx.doi.org/10.1016/ j.egypro.2014.11.458.

Chopra, S., Marfurt, K., 2006. Seismic attributes e a promising aid for geologic prediction. In: CSEG Rec. 2006 Spec. Ed., pp. 110-121.

Chopra, S., Marfurt, K.J., 2007. Seismic Attributes for Prospect Identification and Reservoir Characterization. Geophys. Dev. Ser. No. 11 465. http://dx.doi.org/ 10.1190/1.9781560801900.

Chopra, S., Marfurt, K., 2015. Enhancing Interpretability of Seismic Data with Spectral Decomposition Phase Components 1976-1980.

Chopra, S., Castagna, J., Alexeev, V., 2006. Spectral Decomposition Applications, vols. 367-368.

Connolly, P., 1999. Elastic impedance. Lead. Edge 18, 438-452. http://dx.doi.org/ 10.1190/1.1438307.

Daber, R., Ephrem, D., Carrillat, A., Paddock, D., Randen, T., 2007. Interpreter's Guide to Seismic Attributes, (October).

Eduardo, A., Matos, C., 2013. Characterization of Gas Chimneys in Almada Basin 2 - 4.

Felifel, E.M., Fathy, M., Moneim, A., Araby, E., Haddad, E., Nassar, M., 2014. 1948439 High-Resolution Imaging Integrated Approach to Enhance Pay Count and Turbidites Reservoir Architecture. Offshore Nile Delta, Egypt 20274.

Furre, A., 2013. Overview of Data Released from the Sleipner CO_2 Injection.

Fyfe, J.A., Gregersen, U., Jordt, H., Rundberg, Y., Eidvin, T., Evans, D., Stewart, D., Hovland, M., Andresen, P., 2003. Oligocene to Holocene. In: Evans, D.,Graham, C., Armour, A., Bathurst, P., co-ordinators (Eds.), The Millenium Atlas: Petroleum Geology of the Central and Northern North Sea. The Geological Society of London, London, pp. 279-287.

Galloway, W.E., 1981. Depositional architecture of cenozoic gulf coastal plain fluvial systems. Soc. Econ. Paleontol. Mineral. 127-155.

Galloway, W., Garber, J., Liu, X., Sloan, B., 1993. Sequence stratigraphic and depositional framework of the Cenozoic fill, Central and Northern North Sea Basin. Geol. Soc. http://dx.doi.org/10.1144/0040033.

Gilani, S.F., 2013. The application of data conditioning, frequency decomposition and DHI from RGB colour blending in the Gohta discovery (Barents Sea). First Break 33, 39 - 45.

Graham, a, Lonergan, L., Stoker, M., 2007. Evidence for Late Pleistocene ice stream activity in the Witch Ground Basin, central North Sea, from 3D seismic reflection data. Quat. Sci. Rev. 26, 627-643. http://dx.doi.org/10.1016/j.quascirev.2006.11.004.

Gregersen, U., Johannessen, P.N., 2007. Distribution of the Neogene Utsira Sand and the succeeding deposits in the Viking Graben area, North Sea. Mar. Pet. Geol. 24,591-606. http://dx.doi.org/10.1016/j.marpetgeo.2007.04.006.

Gregersen, U., Michelsen, O., Sørensen, J., 1997. Stratigraphy and facies distribution of the Utsira Formation and the Pliocene sequences in the northern North Sea. Mar. Pet. Geol. 14.

Guo, H., Lewis, S., Marfurt, K.J., 2008. Mapping multiple attributes to three- and four component color models d a tutorial. Geophysics 73, W7. http://dx.doi.org/10.1190/1.2903819.

Hall, M., Trouillot, E., 2004. Predicting stratigraphy with spectral decomposition. In: CSEG Natl. Conv., pp. 1-3.

Haralick, R.M., 1984. Digital step edges from zero crossings of second directional derivatives. In: IEEE Transactions on Pattern Analysis and Machine Intelligence PAMI 6, pp. 58 - 68.

Harrington, J.F., Horseman, S.T., 1999. Gas transport properties of clays and mudrocks. Geol. Soc. Lond. Spec. Publ. 158, 107-124. http://dx.doi.org/10.1144/ gsl.sp.1999.158.01.09.

Hart, B., 2012. An Introduction to Seismic Interpretation. AAPG Disco. In: AAPG Datapages (Ed.), 1444 South Boulder Avenue, Tulsa, OK 7411, USA, Tulsa, OK USA.

Head, M.J., Riding, J.B., Eidvin, T., Chadwick, R.A., 2004. Palynological and foraminiferal biostratigraphy of (Upper Pliocene) Nordland Group mudstones at Sleipner, northern North Sea. Mar. Pet. Geol. 21, 277-297. http://dx.doi.org/ 10.1016/j.marpetgeo.2003.12.002.

Heggland, R., 1997. Detection of gas migration from a deep source by the use of exploration 3D seismic data. Mar. Geol. 137, 41-47.

Henderson, J., Purves, S.J., Leppard, C., 2007. Automated delineation of geological elements from 3D seismic data through analysis of multi-channel, volumetric spectral decomposition data. First Break 25, 87-93.

Holloway, S., Chadwick, R., Kirby, G., 2000a. Saline aquifer CO_2 storage (SACS)-final report: Work area 1 (Geology). BGS Rep. 1, 31.

Holloway, S., Chadwick, R., Kirby, G.A., Pearce, J., Gregersen, U., Johannessen, P.N., Kristensen, L., Zweigel, P., Lothe, A., Arts, R., 2000b. Saline Aquifer CO_2 Storage (SACS2). Final report: Geological characterisation of the Utsira Sand reservoir and caprocks (Work Area1). BGS Rep. 31pp.

Iacopini, D., Butler, R.W.H., Purves, S., 2012. Seismic imaging of thrust faults and structural damage: a visualization workflow for deepwater thrust belts. First Break 30, 77 - 84.

Isaksen, D., Tonstad, K., 1989. A revised Cretaceous and Tertiary lithostratigraphic nomenclature for the Norwegian North Sea. Nor. Pet. Database, Bull. 5.

Iske, A., Randen, T., 2005. Mathematical Methods and Modelling in Hydrocarbon Exploration And Production.

Jackson, C., Stoddart, D., 2005. Temporal constraints on the growth and decay of large-scale mobilized mud masses and implications for fluid flow mapping in sedimentary basins. Terra Nov. 17, 580-585. http://dx.doi.org/10.1111/j.1365-3121.2005.00652.x.

Jordt, H., Faleide, J.I., Bjørlykke, K., Ibrahim, M.T., 1995. Cenozoic sequence stratigraphy of the central and northern North Sea Basin: tectonic development, sediment distribution and provenance areas. Mar. Pet. Geol. 12, 845-879. http://dx.doi.org/10.1016/0264-8172(95)98852-V.

Kragh, E., Christie, P., 2002. Seismic repeatability, normalized rms and predictability. Lead. Edge 640e647. http://dx.doi.org/10.1190/1.1497316.

Kirby, G., Chadwick, R., Holloway, S., 2001. Depth Mapping and characterisation of the Utsira Sand Saline Aquifer, Central and Northern North Sea Depth mapping and characterisation of the Utsira Sand Saline Aquifer, Central and Northern North Sea.

Lindeberg, E., Zweigel, P., Bergmo, P., Ghaderi, A., Lothe, A., 2000. Prediction of CO_2 distribution pattern improved by geology and reservoir simulation and verified by time lapse seismic. SINTEF Petroleum Research, in: Research, S.P. (Ed.),.Conference, Fifth International Gas, Greenhouse Technologies, Control.

Liner, C.L., 2004. Elements of 3-D Seismology. PenWell, 608 p.

Loseth, H., Wensaas, L., Arntsen, B., Hovland, M., 2003. Gas and fluid injection triggering shallow mud mobilization in the Hordaland Group, North Sea. Geol. Soc. Lond. Spec. Publ. http://dx.doi.org/10.1144/gsl.sp.2003.216.01.10.

Løseth, H., Gading, M., Wensaas, L., 2009. Hydrocarbon leakage interpreted on seismic data. Mar. Pet. Geol. 26, 1304-1319. http://dx.doi.org/10.1016/j.marpetgeo.2008.09.008.

Løseth, H.,Wensaas, L., Arntsen, B., Hanken, N.-M., Basire, C., Graue, K., 2011. 1000 M long gas blow-out pipes. Mar. Pet. Geol. 28, 1047-1060. http://dx.doi.org/ 10.1016/j.marpetgeo.2010.10.001.

Mahapatra, S.N., 2006. Determination of heterogeneity by high-resolution seismic reservoir characterization in the heavy oil temblor reservoir of coalinga field, California. Diss. Abstr. Int. Sect. B 66, 5868-B.

Marfurt, K.J., Alves, T.M., 2014. Pitfalls and limitations in seismic attribute interpretation of tectonic features. Interpretation 3, SB5-SB15. http://dx.doi.org/ 10.1190/INT-2014-0122.1.

Marfurt, K.J., Sudhaker, V., Gersztenkorn, A., Crawford, K.D., Nissen, S.E., 1999. Coherency

calculations in the presence of structural dip. Geophysics 64, 104. http://dx.doi.org/10.1190/1.1444508.

Mavko, G., Mukerji, Tapan, Avseth, P., 2010. Techniques for quantitative seismic interpretation. Quant. Seism. Interpret. Rock Phys. Tools Reduce Interpret. Risk 168 - 211. http://dx.doi.org/10.1017/CBO9780511600074.005.

McArdle, N.J., Ackers, M.A., 2012. Understanding seismic thin-bed responses using frequency decomposition and RGB blending. First Break 30, 57 - 65.

Miall, A.D., 1980. Cyclicity and the facies model concept in fluvial deposits. Bull. Can. Pet. Geol. 28, 59-80.

Miall, A.D., 1988. Reservoir heterogeneities in fluvial sandstones: lesson from outcrop studies. Am. Assoc. Pet. Geol. Bull. 72, 682-697. http://dx.doi.org/10.1306/703C8F01-1707 11D7-8645000102C1865D.

Nicoll, G., 2012. Evaluation of the Nordland Group Overburden as an Effective Seal for the Sleipner CO_2 Storage Site (offshore Norway) using Analytical and Stochastic Modelling Techniques. Retrieved from: http://ethos.bl.uk/OrderDetails do?uin¼uk.bl.ethos.578424.

Nicoll, G.D., Naylor, M., Haszeldine, R.S., Cavanagh, A.J., Geiger, S., 2010. Could $C0_2$ storage site performance be compromised by palaeo-gas migration conduits in the overburden?. In: Society of Petroleum Engineers - 72nd European Association of Geoscientists and Engineers Conference and Exhibition 2010-Incorporating SPE EUROPEC 2010, vol. 7, pp. 5482-5483.

Partyka, G., Gridley, J., Lopez, J., 1999. Interpretational applications of spectral decomposition in reservoir characterization. Lead. Edge 18, 353. http:// dx.doi.org/10.1190/1.1438295.

Philips, P.P., Zhang, J., 2009. Combining Seismic Imaging with Geologic Process guided Modelling to Improve Channel Reservoir Characterization, pp. 791-793.

Purves, S., 2014. Phase and the Hilbert transform. Lead. Edge 33, 1164e1166. http:// dx.doi.org/10.1190/tle33101164.1.

Ran, Q.,Wang, Y., Sun, Y., Yan, L., Tong, M., 2014. Internal architecture of volcanic gas reservoirs. Volcan. Gas. Reserv. Charact. 15e75. http://dx.doi.org/10.1016/B978- 0 12-417131-2.00002-8.

Robertson, J.D., Nogami, H., 1984. Complex seismic trace analysis of thin beds. Geophysics 49 (4), 344. http://dx.doi.org/10.1190/1.1441670.

Rundberg, Y., 1989. Tertiary Sedimentary History and Basin Evolution of the Norwegian North Sea between 60^{o} and 62^{o}N - an Integrated Approach.

Satur, N., Hurst, A., 2007. Sand-injection structures in deep-water sandstones from the Ty Formation (Paleocene), Sleipner Øst Field, Norwegian North Sea. Sand Inject. Implic. Hydrocarb. Explor. Prod. 113-117 doi:-.

Sheriff, R.E., Geldart, L.P., 1995. Exploration Seismology, 2nd Ed. Cambridge University Press, New York. 592 pp.

Shukla, R., Ranjith, P., Haque, A., Choi, X., 2010. A review of studies on CO_2 sequestration and caprock integrity. Fuel 89, 2651-2664. http://dx.doi.org/10.1016/j.fuel.2010.05.012.

Taner, M.T., 1979. Complex seismic trace analysis. Geophysics 44, 1041. http://dx.doi.org/10.1190/1.1440994.

Wild, J., Briedis, N., 2010. Structural and stratigraphic relationships of the Palaeocene mounds of the Utsira high. Basin Res. 22, 533 - 547. http://dx.doi.org/10.1111/j.1365 2117.2010.00479.x.

Wu, C., Peng, D., Pang, X., 2007. Study on the microscopic internal architecture of Zhujiang deep water fan system in South China Sea. In: Sediment Geol Tethyan.

Zweigel, P., Arts, R., Lothe, A.E., Lindeberg, E.B.G., 2004. Reservoir geology of the Utsira Formation at the first industrial-scale underground CO_2 storage site (Sleipner area, North Sea). Geol. Soc. Lond. Spec. Publ. 233, 165e180. http://dx.doi.org/10.1144/GSL.SP.2004.233.01.11.

Zweigel, P., Hamborg, M., Arts, R., Lothe, A., Sylta, Ø., Tømmerås, A., 2001. Prediction of migration of CO_2 injected into an underground depository: reservoir geology and Conference on Greenhouse Gas Control Technologies, August 13-16 2000, Cairns, Australia, pp. 360 - 365.

Zweigel, P., Lothe, A.E., Arts, R., Hamborg, M., 2000. Reservoir geology of the storage units in the Sleipner CO_2 - injection case e a contribution to the Saline Aquifer CO_2 Storage (SACS) project. SINTEF Pet. Res. 1e79. Report No: 23.4285.00/02/00.